ACS Catalysis

Review

pubs.acs.org/acscatalysis

Recent Advances on the Design of Group VIII Base-Metal Catalysts with Encapsulated Structures

Hao Tian, Xinyu Li, Liang Zeng, and Jinlong Gong*

Key Laboratory for Green Chemical Technology of Ministry of Education, School of Chemical Engineering and Technology, Tianjin University, Collaborative Innovation Center of Chemical Science and Engineering, Tianjin 300072, China

ABSTRACT: Inexpensive group VIII metal (i.e., Fe, Co, and Ni)-based solid catalysts have been widely used in various energy transformation processes such as Fischer−Tropsch (F−T) synthesis, reforming, and water−gas shift reactions. The emerging encapsulation strategy, which represents active metal species that are coated by a protective shell or matrix, has been demonstrated as a powerful means to promote the catalytic performance (i.e., activity, stability, and selectivity) of Fe-, Co-, and Ni-based catalysts due to synergic effects from the well-defined structures. This review describes recent progress on the design and synthesis of encapsulated group VIII base-metal nanomaterials developed for energy and environmental catalysis including syngas conversion, CO_2 dry reforming, steam reforming, methane conversion, and NH_3 decomposition. We start with an introduction of the catalysts with different encapsulating structures (e.g., core@shell, yolk@shell, core@tube, mesoporous structures, and lamellar structures). Then, the synthetic methods of Fe-, Co-, and Ni-based catalysts with encapsulated structures are described in detail. The functions of encapsulation structures in catalysis, including protecting metal nanoparticles (NPs) from sintering, promoting the activity due to the confinement effect, and intensifying reaction processes in the form of multifunctional catalysts, are discussed, respectively. Our perspectives regarding the challenges and opportunities for future research in the field are also provided.

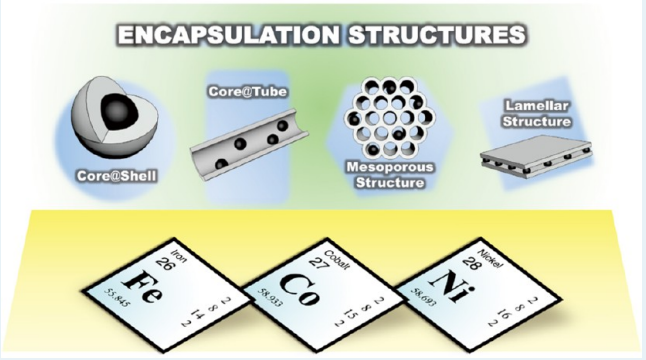

KEYWORDS: *group VIII base metal, iron, cobalt, nickel, encapsulation structure, antisintering, confinement effect, multifunctional catalysts, catalyst design*

1. INTRODUCTION

Heterogeneous catalysts, especially based on metal nanoclusters, perform an irreplaceable role in energy and fuel industries.[1] Among different kinds of metals, noble-metal (e.g., Pt, Rh, and Pd) catalysts have been applied in the production of various fuels and chemicals due to their inherent catalytic capacity.[2−4] However, the scarcity of noble metals strongly demands the development of alternative base-metal catalysts with high-performance catalytic capability. Owing to their electronic properties such as d-band center, the group VIII metal elements in the fourth period, including Fe, Co, and Ni, have been investigated and applied in a variety of important industrial catalytic reactions (Table 1).[5−7] Moreover, Fe-, Co-, and Ni-based catalysts have also been widely applied in energy transformation processes, including Fischer−Tropsch (F−T) synthesis,[8] steam and aqueous reforming,[9] methanation,[10] CO_2 dry reforming,[11] water−gas shift,[12] and CO oxidation.[13] Although these base catalysts have shown great potential in many heterogeneous catalytic reactions, their catalytic properties (e.g., activity, stability, and selectivity) are still not comparable to noble metals. For example, Pt and Ni elements are the most effective metals for catalyzing the cleavage of C−H and C−C bonds in hydrocarbon steam reforming reactions.[9] Compared with Pt-based catalysts, however, Ni reforming catalysts are more prone to deactivation due to the agglomeration of Ni nanoparticles (NPs) and carbon

Table 1. Some Typical Applications of Fe-, Co-, and Ni-Based Heterogeneous Catalysts in Chemical and Fuel Industries[5−7]

catalysts	reactions	existing forms under reaction conditions
Fe-based catalysts	ammonia synthesis	α-Fe
	F−T synthesis	α-Fe, Fe_xC, Fe_xN, Fe_xCN
	water−gas shift reaction	Fe_3O_4
	butane dehydrogenation	α-Fe_2O_3
Co-based catalysts	F−T synthesis	Co, Co_3O_4
	hydroprocessing, hydrodesulfurization, hygrodealkylation and hydrodenitrogenation	Co-MoS_2
Ni-based catalysts	hydrogenation	Raney Ni, Urushibara Ni, Ni
	steam reforming, cracking and hydrotreating	Ni

Received: June 11, 2015
Revised: July 10, 2015
Published: July 14, 2015

DOI: 10.1021/acscatal.5b01221
ACS Catal. 2015, 5, 4959−4977

Scheme 1. Categories of the Catalysts with Encapsulated Structures. Adapted with Permission from Ref 21. Copyright 2014 The Royal Society of Chemistry.[21]

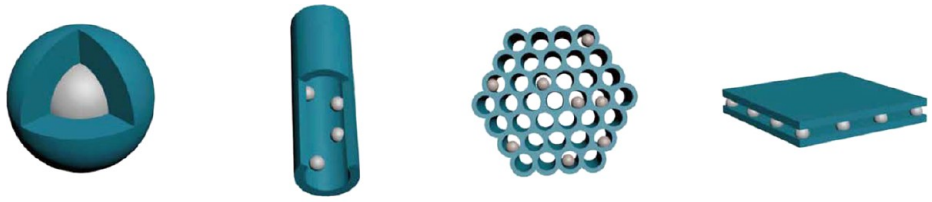

deposition, especially in high-temperature conditions.[14−16] The insufficient catalytic performance of group VIII base metals restrict their large-scale utilizations in more heterogeneous catalytic processes.

The methodologies for rational design of Fe-, Co-, and Ni-based catalysts have been developed rapidly in the past decade with emerging colloidal and surface chemistry, among which the catalysts with encapsulated structures have shown excellent catalytic properties, such as superior activity and thermal stability against sintering.[17−20] Encapsulation strategy is achieved by introducing a coating to stabilize the active metal species in catalysts. The coatings in encapsulated catalysts possess different forms, such as shells, tubes, sheaths, matrices and films. On the basis of the morphology, the catalysts with encapsulation structures can be classified into four groups: (1) core@shell and yolk@shell; (2) core@tube; (3) mesoporous structures and (4) lamellar structures (Scheme 1).[21]

The encapsulation structure not only modulates the catalytic properties of metal NPs but also protects metal NPs from growing larger. It has been reported recently that single Fe sites embedded in a SiO_2 matrix showed prominent catalytic activity and selectivity in the conversion of methane to ethylene and aromatics,[22] indicating that the properties of base-metal catalysts could be upgraded notably by changing the chemical environment of the metal atoms or nanoclusters. Bao and his group used *confinement* to define such modifications of catalytic properties derived from confined space in encapsulation structures.[23,24] However, mass transfer could be hindered by the encapsulation structure to some extent, which is disadvantageous to the catalytic process. This matter should be considered carefully in the design and synthesis of the catalysts with encapsulation structures.

This paper describes recent progress on the rational design of these four types of encapsulated catalysts based on inexpensive group VIII metals. We first introduce the synthesis approaches of encapsulated catalysts according to the morphology classification. The promotion effects on the catalytic performance of Fe-, Co-, and Ni-based catalysts caused by encapsulation structures are then discussed. The relationship between the structure and catalytic performance of encapsulated catalysts are also described. Additionally, we provide perspectives regarding the challenges and opportunities for research involved in the field. It should be noted that catalysts derived from mineral-type compounds, such as perovskites, spinels, and layered double hydroxides, could also provide metal NPs with a confined environment. On account of existing in-depth reviews with respect to the applications of mineral-type materials in catalysis,[25−27] the relevant contents are not discussed in this review.

2. SYNTHESIS METHODS

2.1. Core@Shell and Yolk@Shell Structures. The terminology of core@shell is defined as NPs encapsulated by an outer shell that encloses the NPs in a confined space.[28,29] Yolk@shell is a "core@void@shell" structure, which is similar to the core@shell structure but different in the void space between the core and the shell.[30,31] Constructing core@shell structure has been confirmed to be an efficacious method to improve the performance of metal catalysts.[32−34] Compared with noble-metal-based (e.g., Pt, Au) core@shell structures, it is more challenging to prepare exquisite base metal core@shell structures with size-selected metal cores. Substantial progress has been made in synthesizing base-metal core@shell catalysts in the past decade. Silica, carbon, and zeolite are mostly used as shell building blocks in these core@shell structures, which are discussed as follows.

2.1.1. M@SiO_2 and M@Doped-SiO_2. SiO_2 is the most common shell in the core@shell structures due to the ease in controlling the SiO_2 precursors.[35] With the protection of the SiO_2 shell, the size of metal NPs could be preserved even under severe reaction conditions. To prepare metal@oxide-type core@shell structures, one of the most common pathways is using a microemulsion media combined with the precursors of metal and silica.[29] Takenaka et al. first prepared silica-coated Ni catalysts to improve the high-temperature stability of Ni NPs by using a water-in-oil (W/O) microemulsion and polyoxyethylene (n = 15) cetyl ether as a surfactant.[36,37] Ni^{2+} in the cyclohexane was reduced by adding $N_2H_4{\cdot}H_2O$ into the microemulsion system. Transmission electron microscopy (TEM) images showed Ni cores with diameters less than 5 nm were synthesized and covered with the SiO_2 shells. The silica-coated Ni catalysts exhibited high activity and stability in methane partial oxidation at 700−800 °C.[36] Although the nickel particle size and SiO_2 shell thickness were not tuned in the research, it provided a useful method to prepare Ni-based core@shell catalysts. Furthermore, Schwank and co-workers fabricated Ni@SiO_2 yolk−shell nanocapsules with the SiO_2 shell thickness in the range of 5.1 to 12.4 nm.[38] The lengths of SiO_2 nanocapsules were strongly dependent on the aging time prior to the addition of the silica precursor, hydrazine concentration, and synthesis temperature.[38]

The Stöber method is the benchmark for preparing core@shell structured materials with SiO_2 shells.[39,40] However, SiO_2 shells prepared by the original Stöber method are nonporous, which is detrimental to the applications in catalysis.[41] Pore-generating reagents have thus been employed in the synthetic procedure. Feyen et al. successfully synthesized α-Fe_2O_3@SiO_2 core@shell catalysts with tunable Fe_2O_3 NP sizes based on the Stöber method.[42] Poly(vinylpyrrolidone) (PVP) and cetyltrimethylammonium bromide (CTABr) were introduced in the encapsulation procedure as a dispersant and a pore-generating

DOI: 10.1021/acscatal.5b01221
ACS Catal. 2015, 5, 4959−4977

Table 2. Synthesis Pathways of $M@SiO_2$ (M = Fe, Co, and Ni) Core@Shell and Yolk@Shell Structure

model	method and surfactant	core		shell		refs
		precursor	metal (oxide) particle size/nm	precursor	shell thickness/nm	
$Ni@SiO_2$ core@shell	water-in-oil (W/O) microemulsion; polyoxyethylene (n = 15) cetyl ether	$Ni(NO_3)_2$, reduction by $N_2H_4{\cdot}H_2O$	<5 nm	TEOS	~20 nm	Takenaka et al.[36,37]
Ni@SiO2 core@shell nanotube	W/O microemulsion; polyoxyethylene (n = 10) cetyl ether	$Ni(NO_3)_2$, reduction by $N_2H_4{\cdot}H_2O$	6.6−10.7 nm	TEOS	5.1−12.4 nm	Dahlberg et al.[38]
α-$Fe_2O_3@SiO_2$ core@shell	modified Stöber method	$FeCl_3{\cdot}6H_2O$ with L-lysine	35, 47, and 75 nm	TEOS with PVP and CTABr	~20 nm	Feyen et al.[42]
$Ni@SiO_2$ core@shell	modified Stöber method	$Ni(NO_3)_2{\cdot}6H_2O$, no reduction with PEG	6−45 nm	TEOS with PVP	10−60 nm	Li et al.[43]
$Co@SiO_2$ core@shell	modified Stöber method	$Co(NO_3)_3{\cdot}6H_2O$ with HMT	~10 nm	TEOS with PVP and H_2O_2	5−20 nm	Zeng et al.[45−47]
$Co_3O_4@SiO_2$ core@shell	modified Stöber method	$Co(NO_3)_3{\cdot}6H_2O$ with PVP	~15 nm	TEOS with TMB and CTACl	~40 nm	Karandikar et al.[48]
α-$Fe_2O_3@SiO_2$ core@shell	sonication-assisted Stöber method	$Fe(NO_3)_3{\cdot}9H_2O$ with PVP	30−50 nm	TEOS with C_{18}TMS	~25 nm	Li et al.[49]
$Ni@SiO_2$ yolk@shell	W/O microemulsion with etching; IGEPAL CO-630	$Ni(acac)_2$, reduction by TOP in oleylamine	~3 nm	TMOS with C_{18}TMS	~6 nm	Park et al.[51]
Ni-yolk@$Ni@SiO_2$	W/O microemulsion; IGEPAL CO-630	$Ni(acac)_2$, reduction by TOP in oleylamine	11.7 nm	TEOS	3.3−15.1 nm	Li et al.[52]
$Co@SiO_2$ yolk@shell	W/O microemulsion with etching; IGEPAL CO-630	$Co(acac)_2$ in oleylamine	~14 nm	TMOS with C_{18}TMS	~10 nm	Park et al.[53]
$Ni@SiO_2$ yolk@shell	Stöber method with etching	$Ni(acac)_2$, reduction by PVP in PD	~24 nm	TMOS with C_{18}TMS	~7 nm	Park et al.[54]

Abbreviations: TEOS, tetraethyl orthosilicate; PVP, poly(vinylpyrolidone); CTABr, cetyltetramethylamonium bromide; PEG, polyethylene glycol; HMT, hexamethylenetetramine, TMB, trimethylbenzene; CTACl, cetyltetramethylamonium chloride; C_{18}TMS, octadecyltrimethoxysilane; $Ni(acac)_2$, nickel(II) acetylacetonate; TOP, trioctylphosphine; TMOS, tetramethyl orthosilicate; PD, 1,5-pentanediol.

DOI: 10.1021/acscatal.5b01221
ACS Catal. 2015, 5, 4959−4977

agent, respectively. The α-Fe_2O_3@SiO_2 core@shell catalysts maintained 80% conversion in ammonia decomposition upon 750 °C for 33 h with a space velocity of 120 000 cm^3 g_{cat}^{-1} h^{-1}.[42] Similarly, the addition of PVP and CTABr could also tune the porosity of SiO_2 shells for preparing Ni@SiO_2 for methane conversion.[43,44] In addition, Zeng et al. prepared a series of Co@SiO_2 core@shell catalysts for F−T synthesis.[45−47] Size-controlled Co_3O_4 NPs were obtained by a low-temperature oxidation method.[47] PVP used in the synthesis played a dual role, which facilitated the dispersion of the NPs as well as the formation of more channels in SiO_2 shells.[45] It was also reported on Co_3O_4@SiO_2 that the addition of trimethylbenzene (TMB) could adjust the pore diameter of SiO_2 shells.[48] Otadecyltrimethoxysilane (C_{18}TMS) could also be used to fabricate the pore structure of SiO_2 shells. α-Fe_2O_3@microporous SiO_2 and α-Fe_2O_3@mesoporous SiO_2 were obtained via a sonication-assisted Stöber process with the addition of C_{18}TMS as a pore-generating agent.[49]

Yolk@shell-type metal@SiO_2 materials could also be derived from core@shell structures. By using an acid etching method, the core@shell structure of Ni@SiO_2 synthesized in the W/O microemulsion eventually transformed into a yolk@shell structure.[50] Park et al. synthesized yolk@shell Ni@SiO_2 catalysts, which had small Ni cores with an average diameter of 3 nm via this approach.[51] Tetramethyl orthosilicate (TMOS) was used as the Si source together with C_{18}TMS as a pore-generating agent during the polymerization of silica. The turnover frequency (TOF) of Ni@SiO_2 yolk@shell catalysts reached 6000 h^{-1} in hydrogen-transfer reactions of acetophenone at 150 °C.[51] By using a similar method, an interesting yolk-satellite-shell structured Ni-yolk@Ni@SiO_2 nanocomposite was obtained by varying the shell thickness of Ni@SiO_2 core@shell particles.[52] Co@SiO_2 and Ni@SiO_2 yolk@shell catalysts were also obtained by combining the synthesis of CoO and Ni NPs, the Stöber method and the acid etching treatment, where the average particle sizes of the Co and Ni yolks are about 14 and 24 nm, respectively.[53,54] Specially, the synthesis of Co@SiO_2 yolk@shell catalysts were carried out in a gram-scale.[53]

The typical synthetic methodologies of M@SiO_2 (M = Fe, Co, and Ni) core@shell and yolk@shell structures are summarized in Table 2. The choice of the Si source and the addition of surfactants have a great influence on the size of metal NPs and the thickness of the SiO_2 shell in core@shell and yolk@shell structures. Some surfactants (e.g., PVP, CTABr, and CTACl) not only facilitate the dispersion of the metal cores but also enhance the porosity of the SiO_2 shells. Compared with the microemulsion method, the Stöber method is more facile with tunable synthetic parameters. Hence, the Stöber method is the primary synthesis method to prepare Fe@SiO_2 and Co@SiO_2. However, preparing nanometer-level Ni or NiO NPs directly from aqueous solution is not facile, and the microemulsion method could be adopted to receive better-defined core@shell structures and smaller nickel NPs.

On account of the importance of the metal−support interaction in catalysis, the activity and stability of metal@SiO_2 catalysts could be limited by the weak interaction between metal and silica. Due to its chemical inertness, SiO_2 can barely assist the activation of the reactive molecules. Numerous efforts have been made to promote the catalytic performance of metal@SiO_2, such as the addition of another metal element and the modification of SiO_2. A series of core@shell structured Ni@SiO_2 doped with different metal elements (Co, Cu, Fe, Ba, Ce, and La) were prepared by Li et al.[55] The precursors of doped metals were simultaneously added with $Ni(NO_3)_2{\cdot}6H_2O$ at a Ni/M molar ratio of 10. La-doped Ni@SiO_2 decreased the amount of carbon deposition and exhibited the best performance in methane partial oxidation reaction.[55] The same group also synthesized Co−Ni@SiO_2 core@shell structures for methane partial oxidation.[56] Similarly, Ni@Ni−Mg phyllosilicate (Ni@Ni-Mgphy) core@shell catalysts were derived from the Ni@SiO_2 core@shell structure through the hydrothermal treatment of Ni@SiO_2 with $Mg(NO_3)_2$.[57] Ni@SiO_2 NPs, which were used as precursors of Ni@Ni-Mgphy, were synthesized via the microemulsion method mentioned above.[52,54] The length of hydrothermal treatment time could influence the porosity and basicity of Ni@Ni-Mgphy.[57] The initial CH_4 TOF value of Ni@Ni-Mgphy with 10 h of hydrothermal treatment achieved 56 s^{-1}, which was more than 3 times higher than that of Ni@SiO_2 (17 s^{-1}) at 700 °C. Moreover, La_2O_3 could also be added as a dopant into Ni@SiO_2 core@shell structure.[58] By carbonizing the organic template used in the aqueous solution, Co_3O_4@C-m-SiO_2 (m = mesoporous) composites were prepared by Xie et al.[59] The C-modified SiO_2 channel exhibited hydrophobic properties, which led to a better selectivity to C_5−C_{18} products.[59]

2.1.2. M@Carbon. Apart from SiO_2, carbon can also act as shell materials with added benefits for many organic reaction catalysts because of its hydrophobicity. Noble metals, including Ag, Au, and Pd, encapsulated by carbon shell via the hydrothermal process have been reported by Sun et al.[60] Inspired by these results, Yu et al. successfully synthesized Fe_xO_y@C, Co_xO_y@C, and Ni_xO_y@C using a one-pot hydrothermal hydrolysis−carbonization method.[61] Typically, $Fe(NO_3)_3{\cdot}9H_2O$ and D-glucose monohydrate are used as the sources for Fe and C, respectively. Fe_xO_y@C with a nominal Fe/glucose ratio of 3:5 was obtained by hydrothermal treatment at 80 °C for 24 h. Smooth carbon sphere with a diameter of ∼6 μm were formed after dehydration and aromatization of glucose. Further characterizations indicated that the Fe_xO_y@C spheres consisted of numerous nanorods interconnected in three dimensions (Figure 1). The particle size of Fe_xO_y was ∼7 nm, and the highest loading of iron oxide could reach 22 wt %. The carbon shell was mesoporous with high surface area (189 m^2/g after reduction). Other saccharides such as fructose and sucrose could also be used as the carbon source. The formation mechanism of Fe_xO_y@C sphere was proposed subsequently: under the hydrothermal condition, iron nitrate was transformed to FeOOH and subsequently reduced to Fe_xO_y by the carbonization process of glucose. The Fe_xO_y-in-C nanorods were formed via the combination of Fe_xO_y NPs and small carbonaceous colloids through Coulombic interactions with surface functional groups (i.e., −OH and −C═O). Fe_xO_y@C spheres were finally formed upon self-assembly of Fe_xO_y-in-C nanorods via further intermolecular dehydration following the layer-by-layer growth. The Fe_xO_y@C catalysts performed excellent stability in F−T synthesis. In a 100 h on-stream test, the conversion of CO only dropped slightly from 86% to 76%.[61] Iron catalysts encapsulated by carbon could also be prepared using biomass char as carbon source according to the result from Yan et al.[62] The controllable synthesis of carbon shell with a wider range of thickness, optimum acid property, and tunable pore structure would be the key to design high-performance M@carbon catalysts.

2.1.3. M@Zeolite. Zeolites are recognized as promising supports and catalysts due to their well-defined pore structure

DOI: 10.1021/acscatal.5b01221
ACS Catal. 2015, 5, 4959−4977

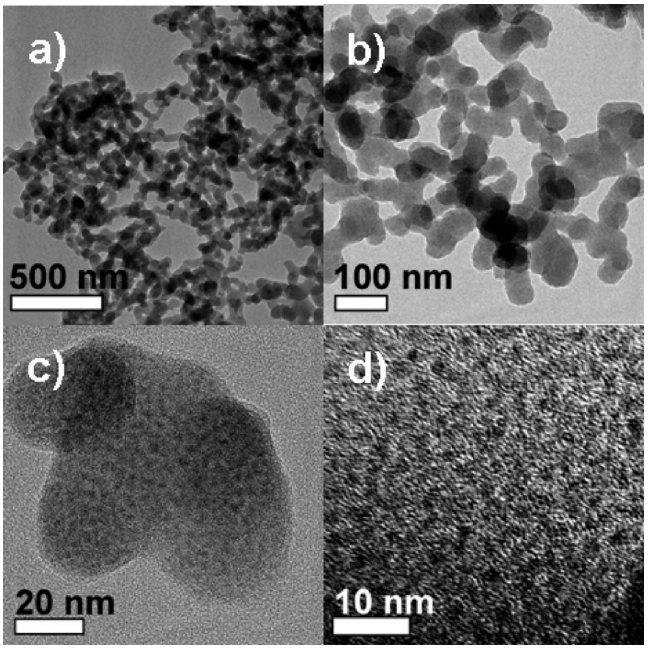

Figure 1. (a−c) TEM images of ground Fe_xO_y@C spheres at different magnifications, showing cross-linked nanorods inside. (d) HRTEM image of one carbonaceous nanorod embedded with iron oxide nanoparticles. Reproduced with permission from ref 61. Copyright 2010 American Chemical Society.[61]

and adjustable acidity. However, the pore sizes of most zeolites are very small, (usually <1 nm), which is not suitable for directly loading metal NPs. Via the agglomeration of ZSM-5 nanorods, Li et al. synthesized Fe_3O_4@ZSM-5 spheres with well-dispersed Fe_3O_4 NPs using an *in situ* crystallization route.[63] Mesoporous silica gel was used as a hard template to confine Fe_3O_4 NPs through a nanocasting and *in situ* glycol-ethylene reduction process. Then, the Fe_3O_4/mesoporous silica gel was utilized as the Si source of ZSM-5. The Fe_3O_4@ZSM-5 spheres were formed after the multistep crystallization of ZSM-5 under the hydrothermal conditions. Aggregated ZSM-5 nanorods formed ZSM-5 spheres with 6−9 μm in diameters. The particle size of Fe_3O_4 NPs was about 10 nm. Good F−T synthesis catalytic performance was observed on the Fe_3O_4@ZSM-5. The catalysts kept over 80% CO conversion after a 110 h reaction, and the selectivity toward C_{13+} products was only 3.2%, which could be attributed to the cracking function of the ZSM-5 shell.[63] Moreover, Ni-based catalysts encapsulated by zeolite shells (MSU-1 and Sil-1) also performed excellent activity in methane steam reforming for hydrogen production.[64,65]

2.2. Core@Tube Structures. Different from core@shell and yolk@shell structures, core@tube composites are materials in which the highly dispersed metal NPs are confined by well-defined channels of nanotubes. Although metal NPs are not encapsulated completely by the wall of nanotube-type support, it has been testified that the core@tube structure also plays a role in suppressing the growth of metal particles and maintaining their sizes at nanometer level. The most typical support in the core@tube form is carbon nanotubes (CNTs). Apart from restricting the sintering of metal NPs, CNTs can also tune the catalytic activity owing to the difference of electronic structure between concave inner-surface and convex outer-surface.[66]

There are several excellent reviews regarding the synthesis of well-dispersed metal or metal oxide NPs inside or outside CNTs.[23,67,68] Herein, we stress the synthetic procedure of Fe, Co, and Ni NPs supported on CNTs. Many techniques have been employed to fill CNT channels with metals, such as arc discharge, vapor deposition, impregnation, and so on.[69−73] Considering the simplicity and universality, the impregnation method is the most suitable approach for catalyst preparation. The preparation of Fe, Co, and Ni NPs inside or outside CNTs could be all achieved via the aqueous process,[74−80] which typically involves the pretreatment of CNTs and the dispersion of metal NPs on CNTs.

CNTs with proper length are essential for a good catalyst support. Channels with a large length/diameter ratio would restrict the mass transport of reactants and products in the nanotubes. Cleavage of CNTs is required once the length of CNTs is beyond several micrometers. The oxidation cleavage of CNTs by a piranha solution (4:1 volume ratio 96% H_2SO_4/30% H_2O_2) has been shown to be effective to pretreat and truncate CNTs with minimal mass loss.[81] Ag and Fe could also catalyze the oxidation cutting process.[68] Additionally, nitric acid is often used to pretreat pristine CNTs.[77,78,82,83] After acid oxidation, functional groups such as −C═O, −COOH, and −O−H appear on the surface of CNTs.[77] By changing the pretreatment conditions, CNTs with open and close ends could be obtained directly. Subsequently, Fe/Co-in-CNTs and Fe/Co-out-CNTs would be derived facilely.[76,84,85] Moreover, nitrogen-doped CNTs, which exhibited superb catalytic performance in F−T synthesis as the support of Fe, could be prepared by a chemical vapor deposition method.[86,87]

Dispersion of metal NPs over CNTs is a crucial step in the synthetic procedure.[88−90] The impregnation method was effective to prepare Co NPs supported on CNTs.[77,79,82] Additionally, the dispersion of Co inside CNTs could be adjusted by introducing the microemulsion environment.[78] Ni NPs inside or outside CNTs with high selectivity by using a facile and reproducible two-stage impregnation method were reported by Su and co-workers.[91] The synthetic procedure is based on the hydrophobicity difference between water and organic solvent. The pore volume of the CNTs was determined by incipient wetness impregnation with water. To prepare Ni NPs inside CNTs, an appropriate amount of ethanol solution with nickel nitrate and water were successively impregnated into CNTs. Subsequently, an appropriate amount of water was then added. For Ni NPs outside CNTs, CNTs were first impregnated with organic solvents and then the aqueous solution with nickel nitrate. The results of 3D-TEM analysis indicated that the selectivities of Ni NPs inside and outside CNTs were 75% and 85%, respectively (Figure 2).[91] This method is convenient to obtain Ni-in-CNTs and Ni-out-CNTs with quantifiable selectivity.

Inorganic nanotubes could also tune the catalytic properties of the metal NPs on the concave inner-surface. One example of Ni-based catalysts is nickel phyllosilicate nanotubes (Ni/PS_n).[92] Ni/PS_n was controllably synthesized via an alkalinity-tuned hydrothermal method (Figure 3). According to the nickel content in the pure phyllosilicate nanotube, the loading of nickel was fixed at 36 wt %. The reduction temperature had a crucial influence on the morphology of Ni/PS_n. With suitable reduction extent, nickel NPs were successfully anchored by the integrated phyllosilicate layered structure. By introducing Ni NPs into PS_n, the nickel size was maintained effectively under an ethanol steam reforming reaction condition, which

DOI: 10.1021/acscatal.5b01221
ACS Catal. 2015, 5, 4959−4977

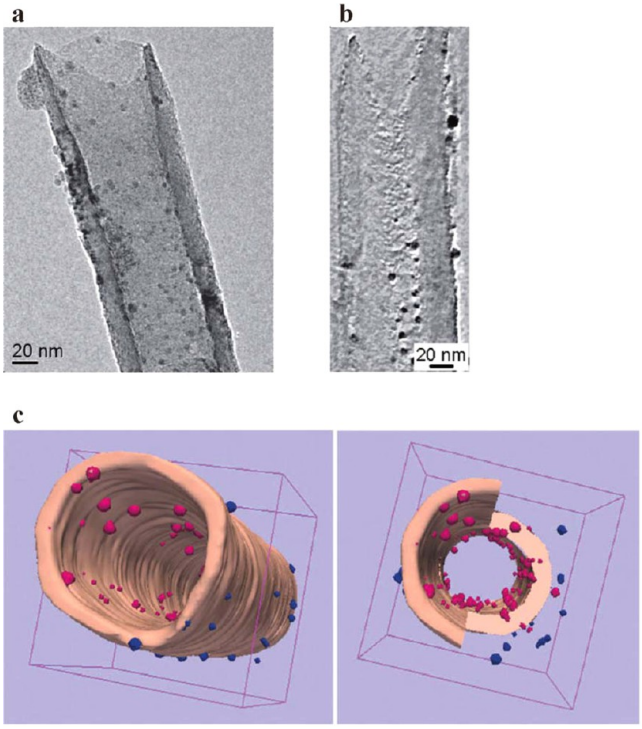

Figure 2. (a) Typical 2D-TEM images of the sample "metal inside", used to reconstruct its volume. (b) Longitudinal section through the reconstructed volume. (c) Modeling of the reconstructed volume: (pink) carbon nanotubes, (red) Ni NPs inside the tube, (blue) Ni NPs on the external surface. Adapted with permission from ref 91. Copyright 2009 American Chemical Society.[91]

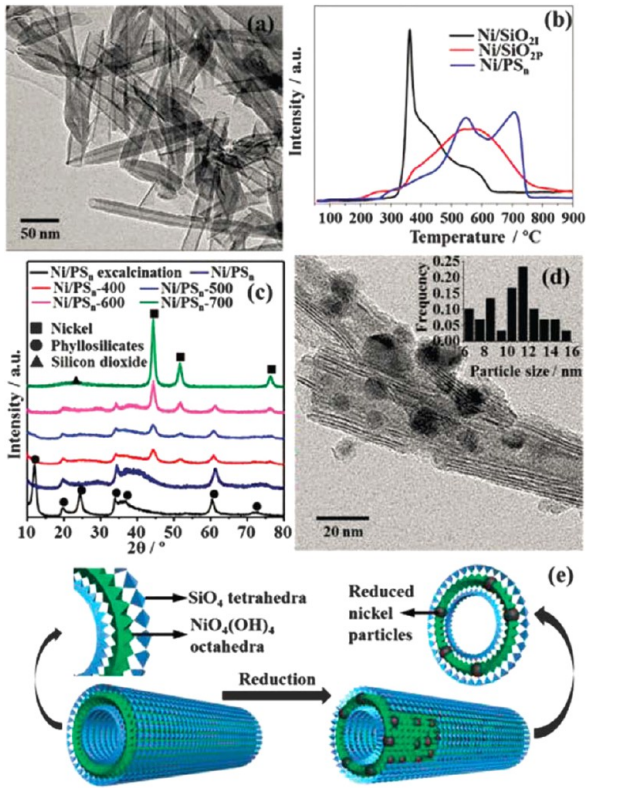

Figure 3. (a) TEM image of the as-prepared Ni/PS_n. (b) TPR profiles of Ni/SiO_2 catalysts. (c) X-ray diffraction (XRD) patterns of Ni/PS_n before and after calcination and upon reduction at different temperatures. (d) TEM image of Ni/PS_n-600. (e) Schematic model of Ni/PS_n and Ni/PS_n after reduction. Reproduced with permission from ref 92. Copyright 2013 The Royal Society of Chemistry.[92]

contributes to the excellent stability of PS_n. The obtained Ni/PS_n after 600 °C reduction kept 90% ethanol conversion after a 100 h ethanol reforming test at 500 °C.[92]

2.3. Mesoporous Structures. Support with suitable pore structures could prevent metal NPs from growing larger as well.[93] The pore structure of the support should meet the following requirements in order to achieve this goal. (1) The pore size distribution should be in a proper range at nanometer level, beyond which the porous support will lose the capacity to restrict the metal NPs from sintering, while below which pores will be exposed to the threats of blockade by metal NPs and of poor mass transfer for reactants and products.[94] (2) Large surface area is a necessity for the support to provide enough pore volume for the loaded metal NPs. (3) The morphology of pores is supposed to connect expediently to outer space to increase the exposed sites of active metals. (4) The pore structure should remain stable at high temperatures. Mesoporous material with well-defined channels is one of the most promising candidates that meet the above criteria. Since the successful synthesis of MCM-41, mesoporous material has attracted wide attention from the catalysis community in the past decade.[95,96]

2.3.1. Mesoporous Silica. MCM-41 and SBA-15 have been well examined among the silica-based mesoporous materials. Previous studies have verified that the introduction of mesoporous silica promotes the catalytic performance of Fe-, Co-, and Ni-based catalysts significantly.[97−103] However, there are still two main problems for existing mesoporous SiO_2. The first one is that the metal dispersion is not always uniform for metal/mesoporous silica composites prepared by the direct impregnation method.[98] The poor dispersion of metal NPs in mesoporous SiO_2 may lead to the blocking of the channels, which greatly reduces the exposed surface area of metal NPs and subsequently lowers the catalytic activity. The other deficiency of silica-based mesoporous materials is the weak interaction between metal NPs and silica, which hampers the stability of the catalysts. For example, the harsh reaction or reduction conditions would induce Ni NPs to move outside mesopores and then sinter.[104]

To solve these problems, the optimization of the impregnation process has been adopted widely to prepare highly dispersed metal NPs loaded in mesoporous channels. Lopes et al. developed a technique to prepare Co_3O_4 NPs confined in SBA-15 by combining organic solvent and aqueous solution to treat ordered mesoporous silica.[105] In the pretreatment process of precursors, dehydrated SBA-15 was suspended in hexane, followed by impregnation with the aqueous solution of cobalt nitrate. This synthetic method prevents Co_3O_4 NPs from dispersing on the external surface of SBA-15.[105−107] Furthermore, the addition of alkane (e.g., hexane) increases the number of germinal and hydrogen-bonded silanol groups, which strengthens the hydrophilicity of SBA-15.[108] Ungureanu et al. reported a simple synthesis approach to confine Cu−Ni NPs in the ordered channels of SBA-15 via incipient wetness impregnation and mild drying (IWI-MD).[109,110] The authors investigated the effect of thermal conditions during the incipient wetness impregnation process (including drying, calcination, and reduction) on the catalyst morphology, and they concluded that drying at room temperature was the key step to achieve high and stable

DOI: 10.1021/acscatal.5b01221
ACS Catal. 2015, 5, 4959−4977

dispersions.[109] Further experiments indicated that, compared with Ni/SBA-15, suitable addition of Cu has a positive effect on the metal dispersion and reducibility.[110] The location and distribution of nickel NPs also have a vital influence on the activity and selectivity of the catalysts.[111] With some careful modifications in synthesis pathways, highly dispersed nickel catalysts could be obtained. One good example was given by de Jong and his co-workers on NiO/SBA-15 system.[112−114] Due to its high solubility and full decomposition at elevated temperatures, nitrate is the most commonly used inorganic precursor. The conversion from $Ni(NO_3)_2$ solution to NiO is a two-step process:[112]

$$3[Ni(OH_2)_6](NO_3)_2(aq) \xrightarrow{T=120^\circ C} Ni_3(NO_3)_2(OH)_4(s) + 4HNO_3(g) + 14H_2O(g)$$

$$Ni_3(NO_3)_2(OH)_4(s) \xrightarrow{T=450^\circ C} 3NiO(s) + 2NO_2(g) + 2H_2O(g) + 1/2O_2(g)$$

With the tool of high angular annular dark field-scanning transmission electron microscopy (HAADF-STEM), the morphology of NiO/SBA-15 under different drying gas flows was obtained (Figure 4). When the thermal decomposition of nickel nitrate was carried out in air, large NiO outside the mesopores could be observed. However, well-dispersed Ni NPs were formed after calcination under NO/He and H_2/He gas flow. Co_3O_4 has similar properties under different gas flows.[112,113] Further research indicated that the presence of NO and H_2 slowed the decomposition rate of $M_x(OH)_y(NO_3)_z$ (M = Ni or Co) and removed the reaction-generated O_2 and NO_2, which favored the sintering and redistribution of NPs in the subsequent calcination process.[112,113] Compared with other hydrated species, the mobility of $M_x(OH)_y(NO_3)_z$ was inhibited markedly, which, in turn, suppressed the growth of NPs.[114] The medium drying temperature (100 °C) could suppress the NPs growth in Co-based ex-nitrate catalysts.[115] In order to achieve high dispersion of Ni NPs, Xie et al. used polyol (e.g., ethylene glycol) as novel delivery conveyors and removable carbon templates in the procedure of Ni/SBA-15 synthesis.[116] Ni^{2+} coordinated with polyol could get into the ordered mesopores of SBA-15 more easily by the capillary force. The polyol then decomposes to carbon during the calcination under N_2 atmosphere. The generated carbon plays a role of protective obstacles, which impedes the migration of Ni NPs from the mesoporous channels to the external. TEM images indicated that small size Ni NPs with uniform distribution were immobilized in mesoporous channels by this ethylene glycol assisted synthesis route. The obtained Ni/SBA-15 catalysts kept active and stable in 20 h CH_4 dry reforming at 750 °C.[116]

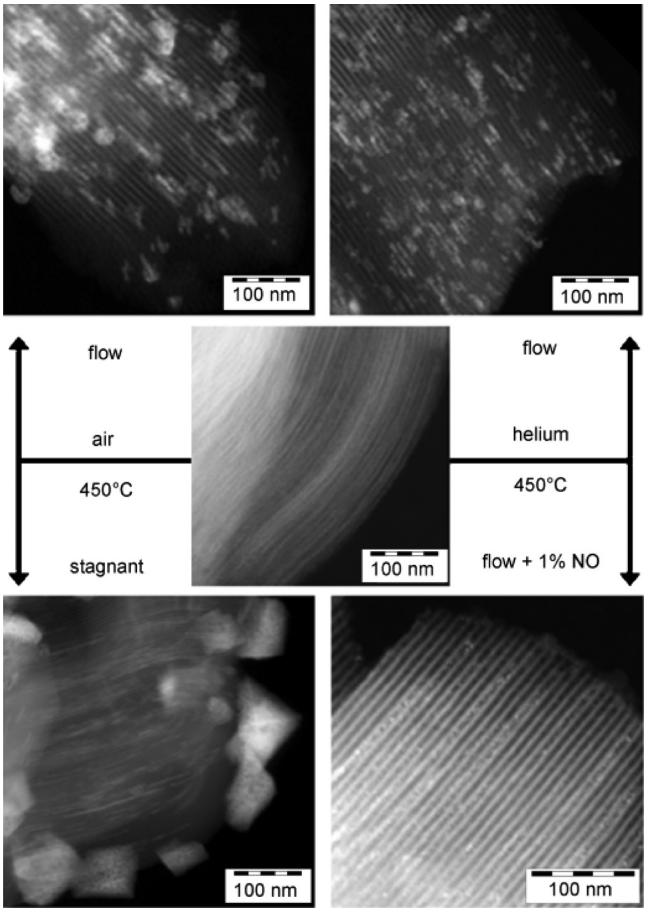

Figure 4. HAADF-STEM images of $Ni_3(NO_3)_2(OH)_4$/SBA-15 obtained after drying at 120 °C (center) and of NiO/SBA-15 obtained after different thermal treatments at 450 °C, as indicated. Reproduced with permission from ref 112. Copyright 2007 John Wiley and Sons.[112]

Besides improving the impregnation method, other efforts have also been made to promote the dispersion of metal NPs and enhance the metal−support interaction, including the changes in the morphology of silica and modifications with some dopants. Yang and co-workers investigated the effects of second metals M (M = Zr, Ti and Mn) on the catalytic performance of Ni-MCM-41 for CO_2 dry reforming.[117] Ni-M-MCM-41 were synthesized by using a conventional hydrothermal method. The dispersion of Ni NPs were improved with the addition of Zr^{4+}.[117] This group also introduced Ni-TUD-1 catalysts into CH_4 dry reforming.[118] Due to the strong anchoring effect of TUD-1, the Ni-TUD-1 prepared by the grafting method achieved high dispersion of nickel NPs and exhibited strong resistance against deactivation in the long term stability test. However, some Ni particles with the size larger than mesopores could be found in TEM images.[118] Ni-KIT-6 was prepared via a one-pot coassembly method by Liu et al.[119] P123 was used as surfactant to direct the coassembly process. The obtained KIT-6 is a kind of mesoporous silica with highly accessible and open pore networks. Compared with the conventional incipient wetness impregnation method, Ni NPs with even dispersion were acquired by using the one-pot coassembly method. One-pot prepared Ni-KIT-6 catalyst performed better activity and stability than Ni/KIT-6 which was prepared via incipient wetness impregnation.[119] Recently, CeO_2-promoted Ni/SBA-15 catalysts were obtained via a surfactant-assisted iso-volumetric impregnation method.[120] Due to the strong interaction between Ni and CeO_2, Ni NPs with small sizes (~5 nm) were homogeneously distributed in the channels of SBA-15. Better H_2 and CO_2 selectivity in ethanol steam reforming were obtained over the Ce-promoted Ni/SBA-15 catalysts.[120] SBA-16, a type of three-dimensional cubic mesoporous silica with cage-like channels and thick pore walls, was used as the support of Ni- and Co-based catalysts.[121,122] Zhang et al. added Ce as dopant to modify the Ni/SBA-16 catalysts for stronger metal−support interaction.[121] Ni and Ce were introduced into SBA-16 by incipient wetness impregnation, and the calcination process was carried out under a He

DOI: 10.1021/acscatal.5b01221
ACS Catal. 2015, 5, 4959−4977

flow. Uniformly sized Ni NPs formed as a result of both the framework of SBA-16 and the strong interaction between Ni and CeO_2. NiCe/SBA-16 kept stable in 100 h CH_4 dry reforming at 700 °C. The reaction-induced collapse of SBA-16 framework was also suppressed by the introduction of Ce.[121] Wang et al. prepared NiMgSBA-15 using a glow discharge plasma treatment.[123] Via the plasma-assisted synthesis method, smaller Ni NPs and stronger Ni−support interaction were obtained. Stronger basic sites also formed on SBA-15 after the plasma treatment. According to the results of thermogravimetric analysis (TGA), temperature-programmed hydrogenation (TPH) and Raman spectra, less graphic carbon species were formed over the plasma-treated NiMgSBA-15 catalyst.[123]

2.3.2. Mesoporous Alumina. Alumina has been widely used as catalyst support in the chemical industry due to its thermal stability and strong interaction with metals.[124] The synthesis of ordered mesoporous alumina is more difficult than silica because of its complicated hydrolysis behavior.[125] Along with the progress in the synthesis of ordered mesoporous alumina with excellent thermal stability via a facile and reproducible evaporation induced self-assembly method (Figure 5),[76] the applications of ordered mesoporous alumina in catalysis have emerged in recent years.[126,127] The typical synthesis method of ordered mesoporous alumina consisted of three steps.[76] Initially, the assembly of Al precursors in ethanol solution by using template agent at room temperature, in which Pluronic P123 (M_{av} = 5800, $EO_{20}PO_{70}EO_{20}$) is often used as template in this process. The solution was then transferred into a 60 °C oven to carry on the ethanol evaporation process for about two or more days. The rate of ethanol evaporation should not be too fast for protecting the mesoporous structure. Finally, the obtained solid was calcined in air at high temperatures to remove the template agent.[76]

The synthetic method of ordered mesoporous alumina was developed to expand its catalytic applications especially in high-temperature reactions. Jaroniec and co-workers extended this synthesis method to the one-pot synthesis of ordered mesoporous alumina supported metal oxides.[128] They substituted Al precursors with metal precursors (Ni, Mg, Ca, Ti, and Cr) by various molar fractions. The characterization results showed that the samples with up to ∼20% of metal oxide still maintained the ordered mesoporous morphology and the metal oxide homogeneously dispersed on the alumina.[128] NiO-Al_2O_3 composites prepared by this method exhibited good catalytic activity and stability in several high-temperature reactions, such as carbon dioxide reforming of methane,[129,130] methane partial oxidation,[131] and methanation.[132] To attain a better catalytic performance of Ni-based catalysts, tricompound composite oxides (i.e., Ni−Mg−Al,[133,134] Ni−Ca−Al,[135,136] Ni−Ce−Al[137,138] and Ni−V−Al[139]) were then prepared using the similar method. Ru was also added to modify the catalytic performance of Ni−Al mesoporous oxides.[140] Typical applications of tricompound Ni-based ordered mesoporous alumina catalysts are summarized in Table 3. Furthermore, Tan et al. synthesized mesoporous γ-alumina supported Ni-MgO via template-free one-pot hydrolysis of inorganic salts.[141−143] The alumina prepared by this method possessed crystalline frameworks and stable structures.[142]

2.3.3. Mesoporous Carbon. Mesoporous carbon with ordered pore structure, such as CMK-typed carbon, is fairly attractive as a support in F−T synthesis over Fe- and Co-based catalysts.[144] There are two general synthetic methods to obtain ordered mesoporous carbon, nanocasting by using ordered

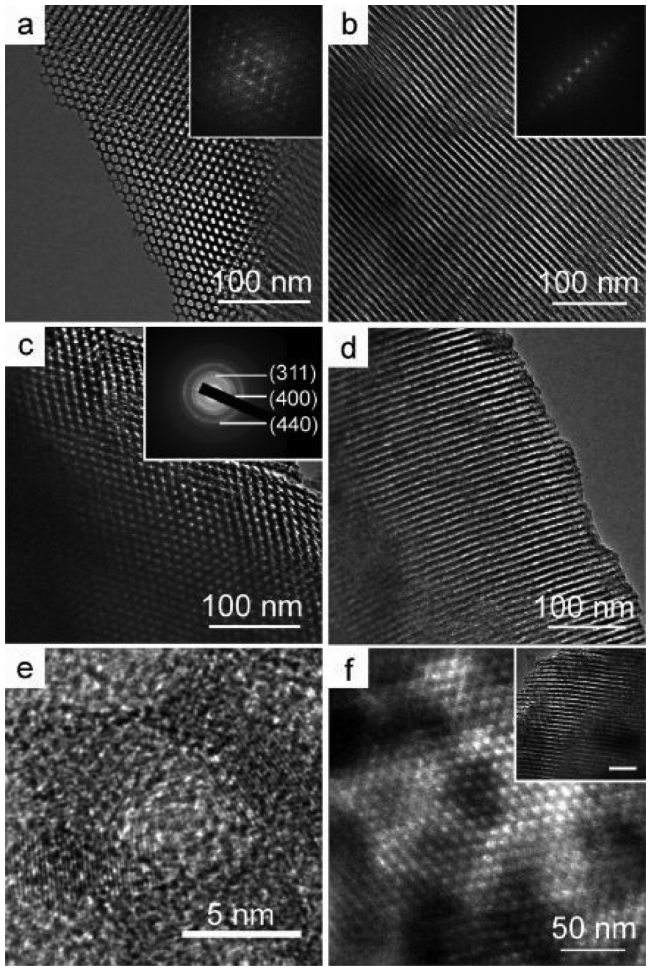

Figure 5. (a) and (b) TEM images of ordered mesoporous alumina calcined at 400 °C viewed along [001] and [110] orientations (fast Fourier transform patterns inset). (c) and (d) TEM images of ordered mesoporous alumina calcined at 900 °C viewed along [001] and [110] orientations (the inset in c is the corresponding selective area electron diffraction pattern). (e) HRTEM image of ordered mesoporous alumina calcined at 900 °C. (f) TEM image of ordered mesoporous alumina calcined at 1000 °C viewed along [001] orientation (the inset is TEM image viewed along [110] orientation). The scale bars are 50 nm for insets. Reproduced with permission from ref 76. Copyright 2008 American Chemical Society.[76]

mesoporous silica (e.g., SBA-15) as hard template and assembly in solution by using nonionic polymer (e.g., F127) as soft template. Impregnation is often used to introduce the metal precursors into the channels of ordered mesoporous carbon.[145,146] Schüth and co-workers successfully synthesized γ-Fe_2O_3/CMK-5 with uniform dispersion (∼6 nm γ-Fe_2O_3 NPs) for ammonia decomposition.[147] Black carbon−silica composites were obtained via a hard template approach. The key point in the synthetic procedure is to impregnate the Fe precursor into the carbon-silica composites, instead of the prepared CMK-5. The thermal treatment was carried out under the Ar atmosphere. γ-Fe_2O_3/CMK-5 achieved 100% NH_3 conversion at 700 °C with a velocity of 60 000 $cm^3\ g_{cat}^{-1}\ h^{-1}$.[147] Zhao and co-workers proposed an ammonia-atmosphere prehydrolysis postsynthetic route to construct high loading (>40%) Fe_2O_3 supported on mesoporous carbon.[148] The crucial step is the *in situ* hydrolysis of $Fe(NO_3)_3{\cdot}9H_2O$ to hydroxides in the mesopores under the NH_3 atmosphere. The

DOI: 10.1021/acscatal.5b01221
ACS Catal. 2015, 5, 4959−4977

Table 3. Typical Applications of Tricompound Ni-Based Ordered Mesoporous Alumina

composition	reaction	temperature	loading amount	activity	stability	references
Ni–Mg–Al	methane steam reforming	500–800 °C	Ni 7 wt %, Mg/(Mg + Al) = 0–20 mol %	78.4% CH_4 conversion at 800 °C, GHSV = 70000 mL/(g·h)	no obvious deactivation at 750 °C for 10 h	Shen et al.[133]
Ni–Mg–Al	CO_2 dry reforming of CH_4	650–800 °C	Ni 10 mol %, Mg 1–10 mol %	94.1% CH_4 conversion at 800 °C, GHSV = 15000 mL/(g·h)	no obvious deactivation at 700 °C for 100 h	Xu et al.[134]
Ni–Ca–Al	CO_2 dry reforming of CH_4	600–800 °C	Ni 5 mol %, Ca 0–10 mol %	~95% CH_4 conversion at 800 °C, GHSV = 15000 mL/(g·h)	no obvious deactivation at 700 °C for 50 h	Xu et al.[135]
Ni–Ca–Al	CO_2 dry reforming of CH_4	700 °C	Ni 5 wt %, Ca/Al = 0–3 mol %	~80% CH_4 conversion at 700 °C, GHSV = 15000 mL/(g·h)	no obvious deactivation at 700 °C for 100 h	Xu et al.[136]
Ni–Ce–Al	CO_2 dry reforming of CH_4	550–800 °C	Ni 7 wt %, Ce/(Ce+Al) = 0–3 mol %	~90% CH_4 conversion at 800 °C, GHSV = 36000 mL/(g·h)	no obvious deactivation at 700 °C for 80 h	Wang et al.[137]
Ni–Ce–Al	CO_2 dry reforming of CH_4	550–800 °C	Ni 7 wt %, Ce/Al = 0–4 mol %	~95% CH_4 conversion at 800 °C, GHSV = 36000 mL/(g·h)	no obvious deactivation at 700 °C for 80 h	Wang et al.[138]
Ni–V–Al	CO methanation	300–450 °C	NiO 10 wt %, V_2O_5 0–7 wt %	74% CH_4 yield at 450 °C, GHSV = 90000 mL/(g·h)	no obvious deactivation at 550 °C for 110 h	Liu et al.[139]
Ru-doped Ni–Al	selective CO methanation	170–330 °C	Ni/(Ni+Al) = 10–50 mol %, Ru 1 wt %	CO was removed from 1 vol % to 10 ppm with more than 50% selectivity for CO methanation, GHSV = 2400 h^{-1}	no obvious deactivation at 200 °C for 200 h	Chen et al.[140]

hydrolysis played a significant role in locating the Fe species inside the channels of mesoporous carbon exclusively.[148] Fe and Co oxides inside ordered mesoporous carbon could also be prepared via a chelate-assisted coassembly soft template approach.[149] By applying phenolic resin as carbon source, metal nitrates as metal sources, acetylacetone (acac) as a chelating agent, and F127 as a template, metal oxides with tunable sizes (Fe_2O_3 NPs from 8.3 to 22.1 nm) confined in ordered mesoporous carbon were obtained after slow evaporation of ethanol and thermal treatment (Figure 6).

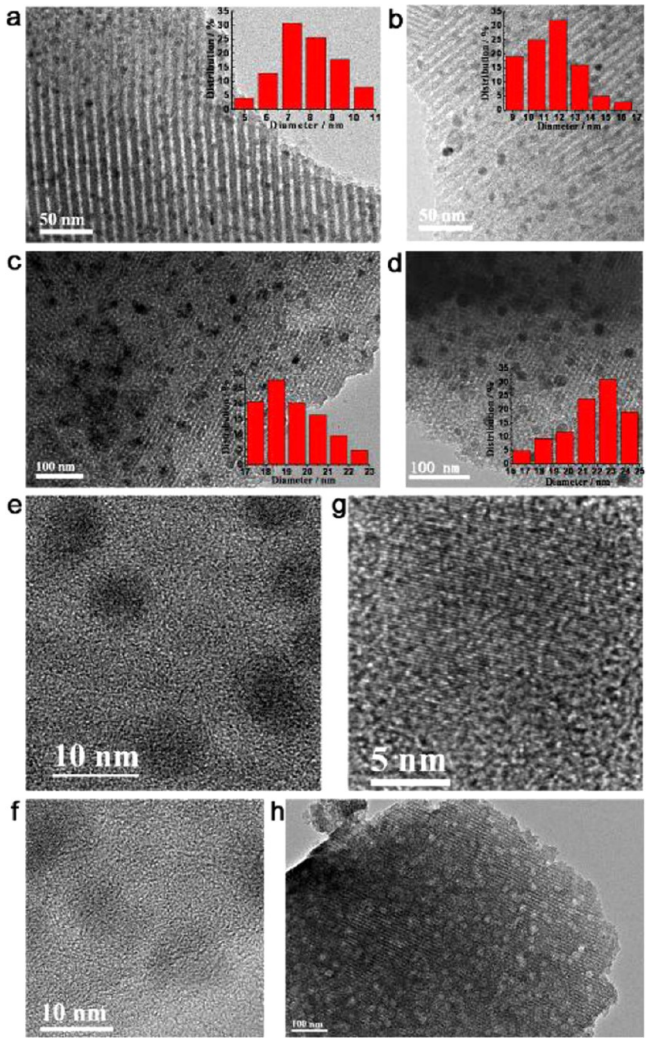

Figure 6. TEM images of the iron-oxide nanoparticles-incorporated ordered mesoporous carbon nanocomposites (Fe–C-z, z refers to grain size/nm of iron-oxide NPs) synthesized with different amount of acac. (a,e) Fe–C-8, (b,f) Fe–C-12, (c) Fe–C-19 and (d,g) Fe–C-22. (h) TEM images of the sample obtained by treating Fe–C-22 with HCl solution, showing uniform nanopores, confirming the embedment of iron-oxide NPs in the carbon wall. Reproduced with permission from ref 149. Copyright 2012 American Chemical Society.[149]

More than 68% C_{5+} selectivity was obtained over the ~8 nm Fe NPs/ordered mesoporous carbon in F–T synthesis.[149] Additionally, nitrogen-doped mesoporous carbon with different N/C ratios could also be obtained by using different nitrogen sources.[150,151]

2.3.4. Other Mesoporous Oxides. Apart from silica, alumina, and carbon, the pore structure of other supports, such as

DOI: 10.1021/acscatal.5b01221
ACS Catal. 2015, 5, 4959–4977

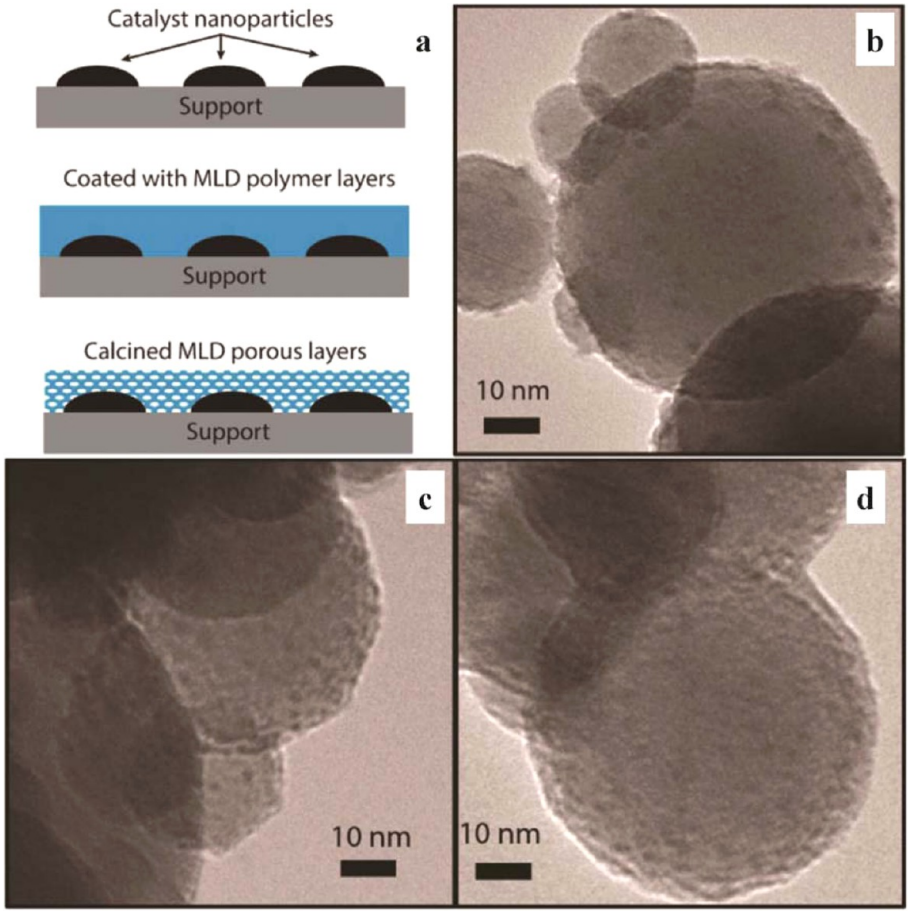

Figure 7. (a) Schematic representation of MLD coating process to produce porous alumina overlayers. (b) Ni nanoparticles (2−5 nm dark particles) deposited on spherical alumina; Ni/Al_2O_3 nanoparticles coated by (c) 5-MLD cycles and (d) 10-MLD cycles. The hybrid polymer−inorganic MLD layer is the lighter layer encircling the spheres in c and d. Reproduced with permission from ref 164. Copyright 2014 American Chemical Society.[164]

zirconia, also has a notable influence on Ni-based catalysts. By introducing Ni NPs into the ZrO_2 matrix, the $Ni@ZrO_2$ nanocomposite was obtained by Li et al. for ethanol steam reforming.[152] Due to the stronger metal−oxide interaction, the novel $Ni@ZrO_2$ nanocomposite exhibited enhanced activity and stability.[152] Sun et al. confirmed that the mesoporous structure of Ni-CaO-ZrO_2 prevented the sintering of Ni NPs effectively in the high-temperature dry reforming process.[153]

2.4. Lamellar Structures. Lamellar structure is another type of well-defined architecture, which can embed metal NPs effectively to offer high surface area and spatial restriction for active sites. Advanced deposition methods, including chemical vapor deposition (CVD),[154] atom layer deposition (ALD),[155−157] and molecular layer deposition (MLD),[158] have been adopted to prepare lamellar-structure-supported catalysts. For example, Lu et al. applied the ALD technique to prepare Pd/Al_2O_3 catalysts with 45 cycles of alumina overcoating for oxidative dehydrogenation of ethane. The ALD-prepared Pd/Al_2O_3 catalysts remained stable with minimal coke formation in a 30 h stability test.[155] Among the different deposition methods, the thickness of the protective oxide overcoat, which has a great influence on the mass transfer of the catalytic reactants, could be precisely controlled by ALD and MLD at a subnanometer level.[159] Sequentially, we introduce the application of ALD and MLD in Ni- and Co-based catalysts synthesis in this section.

By using the ALD method, Kim et al. prepared TiO_2-coated Ni core@shell structure catalysts to compare with bare Ni catalysts without TiO_2 layer.[160] The thickness of the TiO_2 layer was modulated by ALD. With the help of the TiO_2 layer, the formation of graphitic carbon on the Ni surface was effectively suppressed.[161,162] Furthermore, 500-ALD cycles of the TiO_2 layer reduced the sintering of nickel particles and promoted the stability of the Ni-based catalysts. The TiO_2-shell/Ni-core catalysts performed with superior stability in the CO_2 dry reforming reaction at 800 °C for 160 h.[160] Huber and co-workers investigated the synthesis of Co-based catalysts coated with Al_2O_3 and TiO_2 layer using ALD.[163] $Co/\gamma\text{-}Al_2O_3$ and Co/TiO_2 were first prepared by the impregnation method as the substrates of ALD. Unfortunately, due to the formation of cobalt aluminate after calcination, the $Al_2O_3/Co/\gamma\text{-}Al_2O_3$ catalyst was not reducible up to 800 °C. The $TiO_2/Co/TiO_2$ catalyst was prepared and was able to be reduced at 600 °C. Co NPs were coated with 30 cycles of ALD TiO_2 (~1.2 nm). $TiCl_4$ was used as the Ti sources and about 1 g Co/TiO_2 was used as substrate in a typical ALD process. The leaching and sintering of Co NPs during aqueous-phase reactions were prevented by the ALD TiO_2 coating.[163] A recent review on the ALD technique in catalyst design by Huber and co-workers has pointed out that the lifetime of catalysts could be extended effectively with the help of ALD, which is hopeful for the base-metal catalyst to replace the precious-metal catalyst.[156]

DOI: 10.1021/acscatal.5b01221
ACS Catal. 2015, 5, 4959−4977

Gould et al. coated Ni-ALD catalysts for CO_2 dry reforming with a porous alumina layer which was grown by MLD with trimethyl aluminum (TMA), ethanolamine (EA), and maleic anhydride (MA).[164] Ni NPs (~5 nm) were deposited on alumina spheres by ALD in a fluidized bed reactor (Figure 7).[165,166] To understand the relationship between the porous Al_2O_3 film thickness and the catalytic performance, different MLD cycles (5−15) were used in the experiments. Calcination temperature had a remarkable influence on the MLD-prepared Ni-based catalysts. The catalytic activity tests and temperature-programmed oxidation (TPO) results indicated that, although the lower calcination temperature was beneficial to the initial activity, the incomplete decomposition of organic materials containing acidic sites would lead to severe coking troubles and catalyst deactivation.[164] Atypical increasing H_2 uptake was also observed under higher reduction temperatures, which was attributed to both deeper reduction of NiO and the pore expansion of Al_2O_3 MLD film. Several-hour activation periods were required in all the MLD-prepared catalysts. However, the activation period disappeared in the later cycles, indicating that some irreversible changes of catalysts, such as expansion of the Al_2O_3 pores and deeper reduction of NiO under reaction conditions, had occurred in the activation period. The 5-MLD cycle catalyst yielded the highest activity of CO_2 dry reforming in the experiments, and the 10-MLD cycle catalyst remained stable even after repeated calcinations and reductions for 108 h.[164]

3. ENCAPSULATION STRATEGIES FOR CATALYST DESIGN

3.1. Antisintering. Surface structures of metal NPs have a significant influence on the performance of catalysts.[19,167] Compared with larger ones, smaller metal NPs have higher surface-to-volume ratios and more under-coordinated sites, which in turn lead to better activity and selectivity in the catalytic reactions.[168,169] However, metal NPs with small sizes are more prone to growing larger under the harsh reaction conditions due to their high free surface energy.[170,171] Sintering of the active sites in catalysts, especially for base metal catalysts, is one of the most important causes for the catalyst deactivation.[172]

There are two mass-transport mechanisms of the metal sintering process, including particle migration and coalescence, and Ostwald ripening (Scheme 2).[173,174] Particle migration and coalescence contains (1) the random migration of the NPs on the surface of the support and (2) the coalescence among the neighboring NPs. Ostwald ripening is composed of the following: (1) the detachment of the metal atom from one NP to form a monomer (single metal atom or some molecular species); (2) the migration of the monomer from the small NP to a larger one, either through the gas phase or on the surface of the support; and (3) the assembly toward a larger NP.[175] It is still uncertain which mechanism dominates the catalyst sintering under severe industrial operating conditions (e.g., high temperatures and pressures). Many factors directly affect the extent of metal particle sintering, such as temperature, reaction time, components and pressure of the atmosphere, catalyst composition, and support morphology. Among these, reaction temperature has a prominent influence on the sintering of NPs.[172] It is widely accepted that surface atoms become mobile at the Hüttig temperature and the migration of lattices occurs at the Tammann temperature.[176] In previous work, the sintering mechanisms were mostly deduced by using particle size distribution (PSD) data, which is obtained by post-mortem characterization. However, considering the limitations of *ex situ* characterization, it is controversial to obtain information about the sintering mechanistic from the indirect observation method.[177] With the help of advanced *in situ* characterization methods (e.g., *in situ* transmission electron microscopy, *in situ* Mössbauer spectroscopy), the understanding of the sintering mechanism on Ni and Co catalysts has made progress in last several years.[178−182] Although Ostwald ripening and particle migration and coalescence occur simultaneously in most cases, it is widely accepted that Oswald ripening has played a more important role in the sintering process.[178−180] Furthermore, the presence of certain gas molecules (e.g., CO and H_2O) could have a remarkable influence on the sintering behavior of metal NPs.[181−185]

Scheme 2. Schematic Illustration of the Sintering Mechanism

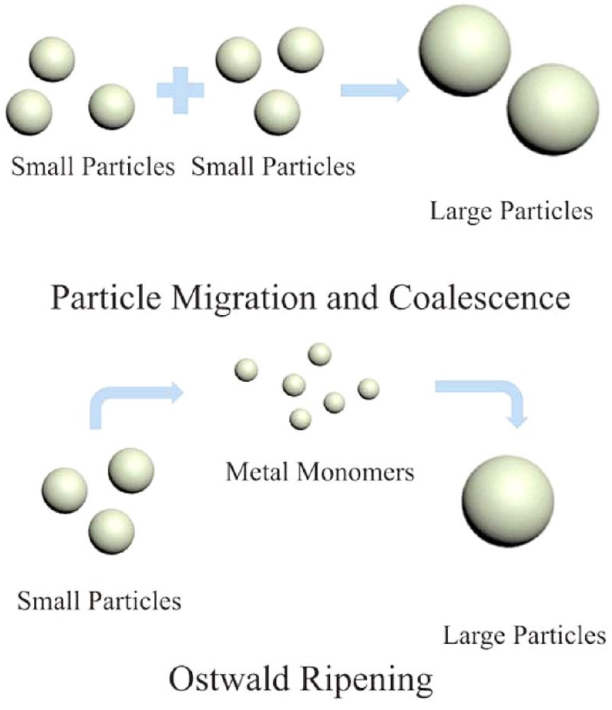

The sintering of metal NPs could be suppressed by encapsulation strategies via the effects of the spatial confinement. With the protection from the coating layer, the transfer of metal monomers or sintering from small NPs to large ones was inhibited. For instance, Pt@SiO_2 core@shell catalysts have been synthesized with excellent stability up to 750 °C.[33] Similarly, most of the Fe, Co and Ni catalysts with encapsulation structures included in this review exhibited antisintering properties to a certain extent. However, the encapsulation structure could be harmful to the catalytic performance. For example, the shells in the encapsulation structures sometimes have a hampering effect on the transport of reactants, which limit the overall reaction rate of the catalytic process. Parameters of the encapsulation structures, such as the thickness of the shells, the size of the metal NPs, and the morphology of the catalysts, have a significant influence on the antisintering ability of the catalysts. Herein, some detailed cases on the understanding of the relationship between encapsulation structure and antisintering property are discussed below.

DOI: 10.1021/acscatal.5b01221
ACS Catal. 2015, 5, 4959−4977

The shell thickness directly affects its protective role to confine metal NPs, and its optimization is a necessity to achieve highly active and stable catalysts with encapsulation structures. Kawi and co-workers studied how SiO_2 shell thickness affected the core@shell structures of Ni@SiO_2 and its catalytic performance in CO_2 dry reforming.[52] All the Ni@SiO_2 catalysts had Ni cores with uniform size of 11.7 ± 1.8 nm in diameter, which made the catalysts with different shell thickness more comparable. The shell thicknesses of SiO_2 were tuned by changing the amount of TEOS and its hydrolysis time. Five different SiO_2 shell thickness (3.3 ± 2.2, 5.7 ± 3.2, 8.6 ± 2.5, 11.2 ± 3.1, and 15.1 ± 2.9 nm) were obtained in the experiment. The authors found that the formation of Ni-yolk@Ni@SiO_2 is dependent on the shell thickness of SiO_2: when the SiO_2 shell thickness reached 11.2 nm, the Ni-yolk@Ni@SiO_2 structure formed. Furthermore, the Ni-yolk@Ni@SiO_2 with 11.2 nm SiO_2 shell thickness possessed the highest Ni dispersion (0.219%) and initial TOF value (79 s^{-1}) of CH_4 among the five catalysts. Because of the insufficient SiO_2 shell thickness, Ni sintering and carbon deposition occurred for the 3.3 and 5.7 nm shell thickness catalysts. Ni-yolk@Ni@SiO_2 with 15.1 nm shell thickness also exhibited instability in CO_2 dry reforming due to severe cross-linking between NPs (Figure 8). The porosity of the SiO_2 shell, Ni species, and reducibility properties were also determined by the thickness of SiO_2 shell.[52]

The degree of size discrepancy between metal NPs and the coatings also has a significant influence on the catalytic performance. If the sizes of metal NPs match the cavities exactly, namely, the metal NPs are totally encapsulated by the coatings, the exposed metal surface and the transport of reactants would be restricted. In comparison, when the sizes of metal NPs were much less than the sizes of cavity, effective spatial restriction cannot be formed. Munnik et al. drew the relationship between Ni NPs growth via the Oswald ripening and Ni particle sizes by using a mesoporous silica support.[94] Ni NPs with different sizes (about 3, 4, 8, and 9 nm, respectively) and spatial distributions were obtained by adjusting the conditions of impregnation, drying, and calcination (Figure 9). The methanation reaction was carried out at 230 °C under H_2 and CO (H_2:CO = 2:1, 1 bar). The mechanism of Ni particles growth under such conditions was dominated by Oswald ripening, which occurred through the formation of $[Ni(CO)_4]$. After a 150 h on-stream test, 3−4 nm Ni NPs were found to grow much larger, and the average particle size reached 20 nm. Some Ni particles with around 100 nm diameter could be found in TEM images. By contrast, only a tiny particle growth was observed on medium sized Ni NPs, from 7.5 to 9.0 nm and 9.0 to 11.0 nm, respectively (Figure 10). The different extents of Ni NPs growth could be explained by supersaturation, which was calculated as the area-weighted average of the Kelvin-like factor $\exp(\lambda/R)$ calculated over all the particles. According to the calculation, the nickel carbonyl supersaturation of small Ni NPs was high enough to break pores of support and grow larger. In contrast, given that the pore size of support was close to the diameter of Ni NPs, supersaturation of medium-sized Ni NPs was limited, which further contributed to the antisintering property of medium sized Ni NPs. This work indicated that the nanometer-level difference in size could determine the distinct performance of catalytic materials.[94]

3.2. Confinement Effect. It has been widely recognized that the electronic structure of metal surfaces is the origin of the

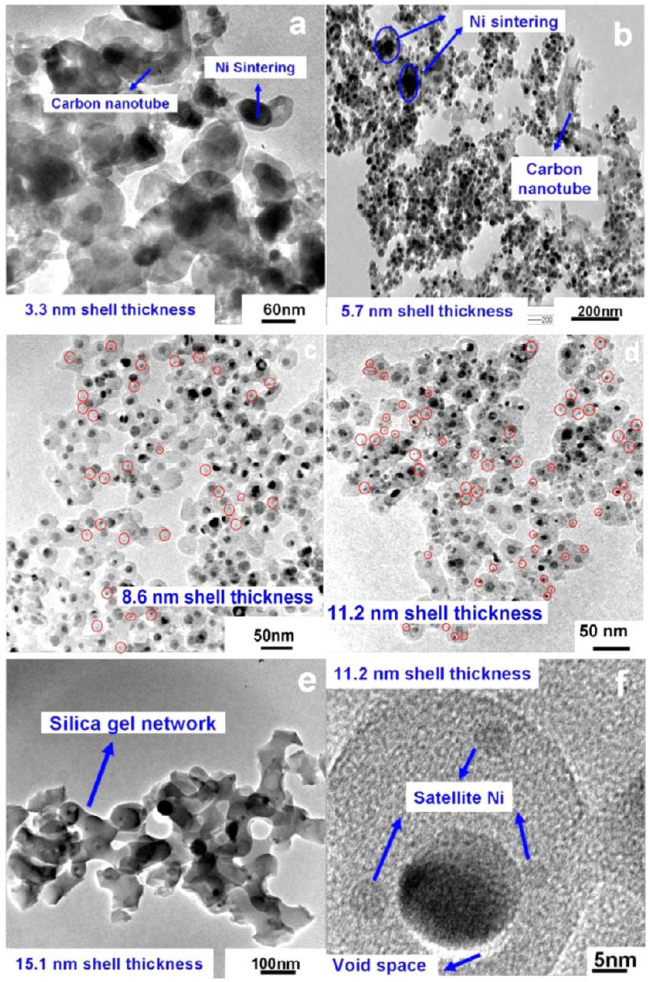

Figure 8. TEM images of spent catalysts with different shell thicknesses after 20 h of reaction: (a−e) low magnification and (f) high magnification for Ni-yolk@Ni@SiO_2 with 11.2 nm shell thickness. Reproduced with permission from ref 52. Copyright 2014 American Chemical Society.[52]

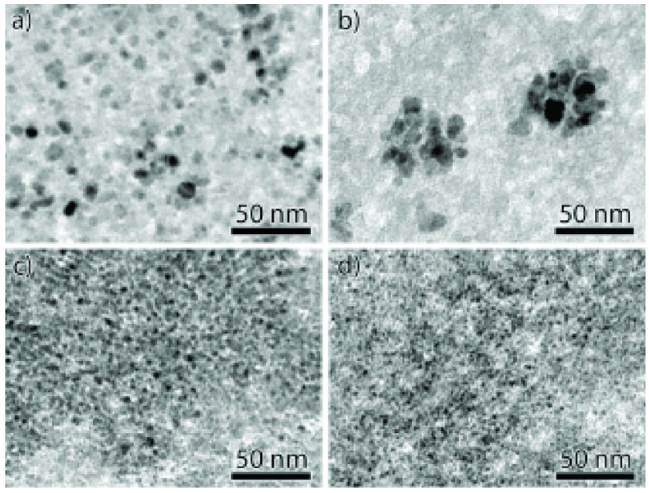

Figure 9. Bright-field TEM of 50 nm thick slices of Ni/SiO_2 catalysts after reduction: (a) Ni-D8, (b) Ni−C9, (c) Ni−C4, and (d) Ni−C3 (C = closer, D = dispersed, the number refers to grain size/nm of Ni NPs before reaction). Reproduced with permission from ref 94. Copyright 2014 John Wiley and Sons.[94]

DOI: 10.1021/acscatal.5b01221
ACS Catal. 2015, 5, 4959−4977

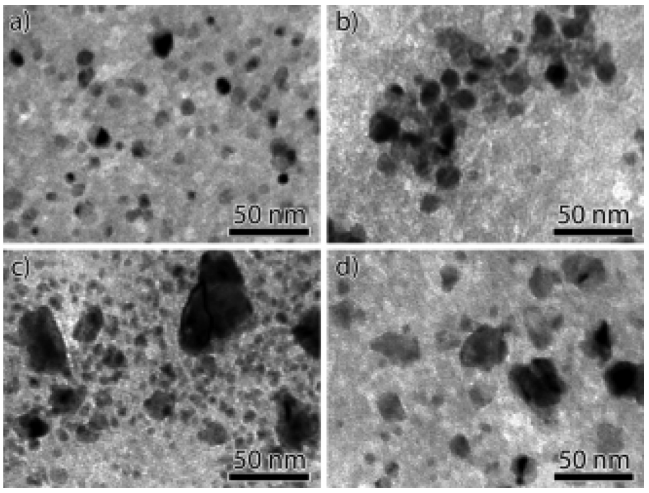

Figure 10. TEM of microtomed 50 nm slices of catalyst particles after 50 h on-stream. (a) Ni-D8, (b) Ni−C9, (c) Ni−C4, and (d) Ni−C3 (C = closer, D = dispersed, the number refers to grain size/nm of Ni NPs before reaction). Reproduced with permission from ref 94. Copyright 2014 John Wiley and Sons.[94]

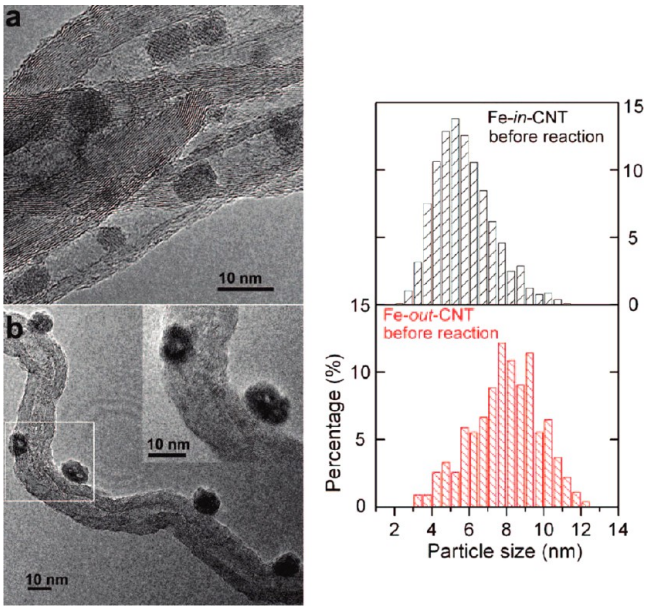

Figure 11. TEM images and particle size distribution of activated catalysts (a) Fe-*in*-CNT and (b) Fe-*out*-CNT before reaction. Reproduced with permission from ref 76. Copyright 2008 American Chemical Society.[76]

catalytic activity.[186−188] Thus, understanding and modulating the electronic structures of metal catalysts are the long-term goals in the field of catalysis and surface science. The metal−support interaction with different intensity in metal catalysts has been found to show different catalytic properties.[189,190] For example, due to the strong interaction between Ni and TiO_x ($x < 2$), TiO_2-supported and SiO_2-supported Ni catalysts exhibited quite different product selectivities in CO hydrogenation.[191] This phenomenon could be attributed to the change in the electronic states of metal NPs caused by the electron transport between metal NPs and supports.[192] In the last 10 years, many researchers have found that the chemical environment of the metal NPs encapsulated by coatings could be modulated by the electronic effects from some specific supports in the encapsulation structure, of which tubular CNTs are mostly used as function supports.[23,67,193] CNT is a member of fullerene structural carbons, which is in the form of reeling graphene layers. Due to the different π electron density caused by the tubular structure, the electronic properties are quite different between inner and outer surfaces of CNTs.[194−196] Therefore, metal NPs inside CNTs and outside CNTs could exhibit different catalytic properties toward specific reactions. As mentioned in the Introduction section, this fine-tuning effect of metal NPs' catalytic properties is termed as the confinement effect in catalysis literature.[73,84,197,198]

Many efforts and progress have been made to discover and understand the difference between redox and catalytic properties of Fe-based NPs inside and outside CNTs by Bao and coworkers.[66,75,76,199−201] The different redox properties between iron oxide inside and outside CNTs were observed and confirmed by *in situ* TEM, CO temperature-programmed desorption (TPD), and XRD.[74] It was found that the reduction temperature of Fe_2O_3 NPs inside CNTs was about 200 °C lower than the ones on the outer surface of CNTs.[74] By using Raman spectroscopy, the abnormal blue shift of Fe−O modes occurred when the Fe_2O_3 NPs were inside the channels of CNTs, which indicated the properties of Fe_2O_3 NPs inside CNTs have been tuned.[199] Then the Fe-*in*-CNTs and the Fe-*out*-CNTs were tested in the F−T synthesis reaction to compare their catalytic performance (Figure 11).[76] The yield of C_{5+} hydrocarbons over Fe-*in*-CNTs was about twice that of Fe-*out*-CNTs. The different catalytic activity could mainly be attributed to the formation of more iron carbides inside CNTs, which have been considered as active species to catalyze F−T synthesis.[76] To further understand the interactions between Fe species and CNTs, theoretical calculations by DFT was employed to study Fe-*in*-CNTs and Fe-*out*-CNTs.[66,200] By constructing the models of Fe atom, Fe_2 dimer, one-dimension Fe nanowire, and one-dimension FeO placed on the inner and outer surface of CNT, it was found that the bondings between the outer surface of CNT and all Fe species were stronger mainly due to the fact that more electrons were distributed on the outer surface.[200] Moreover, comparing to the metal clusters on the outer surface, the d-band states of metal clusters encapsulated by CNT were downshifted, which meant the binding between reactive molecules and metal clusters inside CNT was weakened due to electronic effects from CNT.[66] Therefore, catalytic activities of the metals with higher binding energy, such as Fe and CO, were promoted by the confinement effect of CNTs. To describe the electronic effects caused by CNTs, the concept of the confinement effect E_{con} was defined as[66]

$$E_{con} = E_b(\text{in}) - E_b(\text{out})$$

The E_b(in) and E_b(out) are binding energies of molecules over the metallic cluster on the inner and outer surface of CNT, respectively. Some catalytic properties of metal/CNTs catalysts are well predicted by applying the concept of the confinement energy (Figure 12).[66] Besides Fe/CNTs, other CNTs supported group VIII base-metal catalysts, including Co/CNTs,[202] Ni/CNTs,[80,203] FeCo/CNTs,[204] and FeN/CNTs,[201] have also shown enhanced catalytic performance due to the confinement effect of CNTs. It should be noted that the confinement effect of CNTs could fail in tuning the catalytic properties for certain cases. Zhu et al. prepared Co NPs in or out multiwalled CNTs (Co-in-MWCNTs and Co-out-CNTs) to discover the relationship between the F−T

DOI: 10.1021/acscatal.5b01221
ACS Catal. 2015, 5, 4959−4977

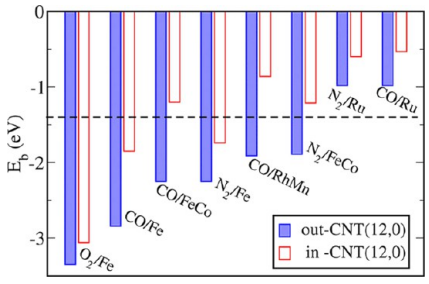

Figure 12. Dissociate binding energies of CO, N_2, and O_2 molecules on typical transition metal clusters (Fe, FeCo, RhMn, and Ru) encapsulated within perfect CNT (12, 0) in comparison to those located on the exterior walls, denoted as in-CNT (12, 0) and out-CNT (12, 0), respectively. The optimal $E_b(CO)$ and $E_b(N_2)$ for CO hydrogenation and ammonia synthesis, obtained from the microkinetic model, is indicated by the dashed line for comparison. Reproduced with permission from ref 66. Copyright 2014 American Chemical Society.[66]

synthesis catalytic performance and the location of cobalt.[85] It was found that the selectivity of C_{5+} products was mainly determined by the activation temperature and the surface chemistry of Co NPs. When the Co-in-MWCNTs and Co-out-MWCNTs were pretreated at 400 °C, no significant differences on the selectivity were observed. The results indicated that the different electronic properties between the inner and outer surface of CNTs did not work on adjusting the F−T synthesis catalytic properties of Co/MWCNTs.[85]

The CNT is not the unique support that has the confinement effect. It has been reported that the Fe confined in the SiO_2 matrix exhibited superior activity and selectivity in nonoxidative conversion of methane.[22] Fe existed in the form of SiO_2 lattice-confined single Fe sites in the 0.5% Fe©SiO_2 catalysts, according to the evidence from HAADF-STEM and *in situ* X-ray absorption near-edge spectroscopy (XANES). The 0.5% Fe©SiO_2 exhibited superior catalytic performance in methane conversion, with a maximum CH_4 conversion of 48.1% and C_2H_4 selectivity of 48.4%. DFT calculations further confirmed that the $\cdot CH_3$ radicals generated on the single Fe sites confined in silica matrix were prone to leaving the surface of Fe instead of undergoing deeper dehydrogenation or C−C coupling.[22] This finding indicated that the catalytic properties may change dramatically when metal sites were encapsulated, or in other words, coordinated with the support at atomic level. Therefore, more efforts are still needed to further understand the confinement effect to promote the catalytic performance of Fe-, Co-, and Ni-based catalysts in the future. Both advanced experimental and theoretical tools will help us to study the confinement effect at subnanometer and even atom level.

3.3. Multifunctional Catalysts. Process intensification is the terminology in the field of chemical engineering to describe the approaches of conducting unit operations in small volume equipment to promote the process efficiency. In other words, obtaining the same amount of desired products with reduced reactor volume and simplified procedures is the primary goal in reaction engineering.[205] It has been found that the catalysts with multiple functions, including the accelerations of tandem reactions, the reinforcements of adsorption process, and the intensifications of mass and heat transfer, could achieve optimum yields of target products.[206−208]

Consecutive reaction (A → B→ C) could be achieved over the catalysts which possess two different active sites for the reaction A → B and B → C, respectively.[32,209] By choosing catalytic-assisted materials as the protective shell, the catalysts with encapsulation structure facilitate the reaction with a dual function. For example, dimethyl ether (DME) has been successfully one-step synthesized from syngas via a novel H-ZSM-5/Cu-ZnO-Al_2O_3 capsule catalyst.[209] The synthesis of methanol from syngas and the further methanol dehydration were achieved consecutively on such encapsulated catalysts.[209]

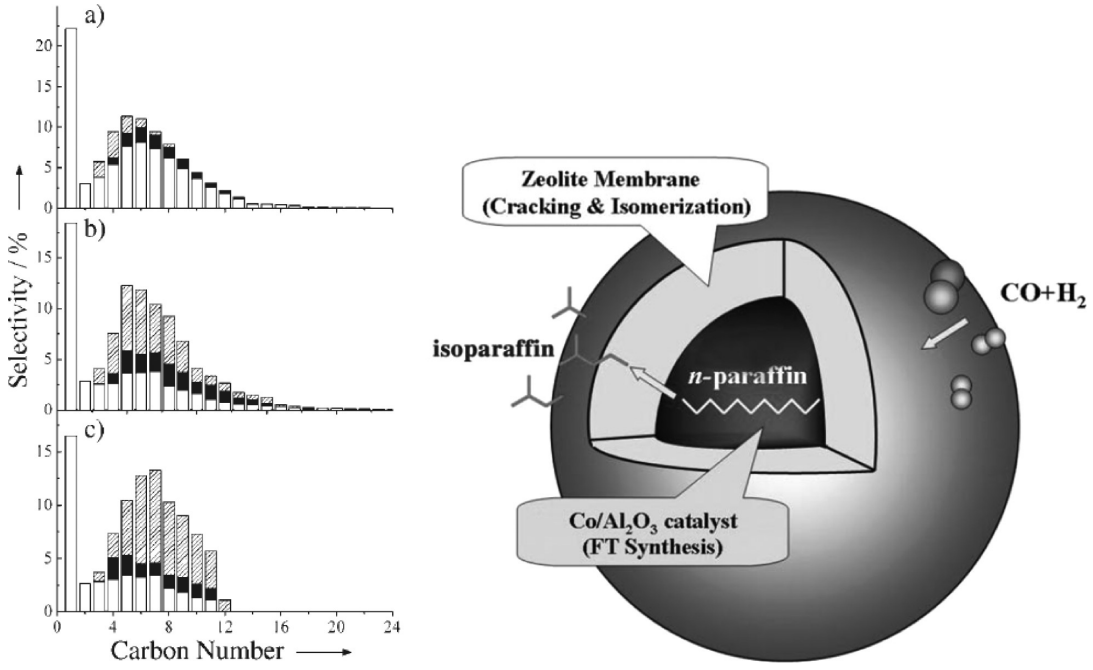

Figure 13. Left are the product distributions for (a) conventional Co/Al_2O_3, (b) the physical mixture of Co/Al_2O_3 and beta-zeolite, and (c) the zeolite-coated Co/Al_2O_3 catalyst. □ = *n*-paraffin, ■ = olefin, hatched = isoparaffin. The right is the model of the core@shell catalyst. Reproduced with permission from ref 32. Copyright 2008 John Wiley and Sons.[32]

DOI: 10.1021/acscatal.5b01221
ACS Catal. 2015, 5, 4959−4977

In this case, the encapsulation structures can be considered as a nanoreactor according to its effects of spatial restriction. The Cu-ZnO-Al_2O_3 core acted as the active site of CO hydrogenation to methanol, and the H-ZSM-5 coating catalyzed the transformation from methanol to DME. In this way, the catalysts with encapsulation structures could achieve bifunctional acceleration of two reactions. Moreover, compared with physical methods to mix two types of active sites in macroscope, the bifunctional encapsulated catalysts exhibit better catalytic performance due to its well-tailored microscopic structures.[210]

One case study is the application of encapsulated Fe- and Co-based catalysts in F−T synthesis.[211] In order to obtain liquid fuels directly, it is significant to reduce the formation of C_{12+} hydrocarbons in F−T synthesis. By combining the CO hydrogenation, acid-catalyzed cracking, and isomerization, bifunctional catalysts consisting of active metal elements (i.e., Co, Fe) and zeolite with encapsulation structure have been proved to be effective to promote the selectivity of C_5−C_{11} hydrocarbons.[32,63,212−215] Tsubaki and co-workers designed Co/Al_2O_3@H-beta zeolite membrane core@shell catalysts to promote the selectivity of middle isoparaffins in F−T synthesis (Figure 13).[32] Under the reaction conditions, CO and H_2 passed through the zeolite membrane and were converted into normal paraffins over Co/Al_2O_3 cores. The generated straight-chain hydrocarbons should pass through the zeolite membrane before they left the catalysts. The cracking and isomerization reactions could take place at the H-beta zeolite. Moreover, the residence time in the core@shell catalysts of straight-chain hydrocarbons with more carbon atoms was longer, which meant the cracking and isomerization of longer isoparaffiins were more likely to be catalyzed by H-beta zeolite in the Co-based catalysts with encapsulation structure.[32] The bifunctional nanoreactor composed of Fe and zeolite has also been applied in the F−T synthesis reaction to achieve selective synthesis of liquid fuels in one-pot synthesis.[216,217] Additionally, the nanoreactor with encapsulation structures could also enrich some reactant molecules inside the catalysts according to the theoretical calculation.[218] The above cases indicated that the encapsulation structures could function as the nanoreactor to intensify the process with improved yield of the desired products.

The performance of encapsulated catalysts could also be promoted by the synergistic effects between the active cores and functional protective layers. Neal et al. prepared Fe_2O_3@$La_{0.8}Sr_{0.2}FeO_{3-\delta}$ core@shell catalysts for methane partial oxidation.[219] The methane partial oxidation was carried out by applying an autothermal chemical looping reforming (CLR) process which consisted of methane reforming and regeneration of catalysts. The syngas yield of Fe_2O_3@$La_{0.8}Sr_{0.2}FeO_{3-\delta}$ core@shell catalysts was about 20% better than that of the Fe_2O_3 and $La_{1-x}Sr_xFeO_{3-\delta}$ nanocomposite. The Fe_2O_3@$La_{0.8}Sr_{0.2}FeO_{3-\delta}$ core@shell catalysts also remained active even after 50 cycles. The concentration of surface oxygen species has a remarkable effect on the catalysts in chemical looping process.[220] The core@shell structure facilitates the diffusivity of O^{2-} and the availability of bulk O^{2-}. Therefore, the better catalytic performance of Fe_2O_3@$La_{0.8}Sr_{0.2}FeO_{3-\delta}$ core@shell catalyst could be attributed to its high-temperature stability and synergistic ionic-electronic conductivity, which improved the transport of lattice oxide between Fe_2O_3 core and $La_{0.8}Sr_{0.2}FeO_{3-\delta}$ shell.[219] The surface properties of the protective shell also play a synergistic role to promote the catalytic properties of encapsulated catalysts. For example, the basicity of Ni-Mgphy enhanced the CO_2 chemisorption and reverse carbon disproportionation reaction ($C + CO_2 \rightarrow 2CO$) in CH_4 dry reforming, which subsequently promoted the activity and stability of the Ni@Ni-Mgphy core@shell catalysts.[57] Moreover, due to the hydrophobic nature, a carbon protective shell has been demonstrated to facilitate the formation of C_{5+} products in Fe- and Co-based catalysts with encapsulation structure in F−T synthesis.[61,146,149]

4. PERSPECTIVES

Encapsulation strategy has been regarded as an efficacious method to promote the catalytic performance of group VIII base metal catalysts. The diverse synthesis methods of Fe-, Co-, and Ni-based catalysts have been developed in recent years. The function of encapsulated catalysts has been investigated widely: (1) the sintering of metal NPs at elevated temperatures could be suppressed by the encapsulation structure via insulating metal NPs in a confined space to diminish their mutual interaction; (2) the binding energy between metal NPs and reactive molecules could also be tuned with the presence of specific encapsulation structures; (3) the yield of products from consecutive reaction could also be elevated with the aid of integrating two different types of active sites. Indeed, the group VIII metal-based catalysts could be promoted effectively by introducing the encapsulation structures. Although the encapsulation strategy has shown its potential to promote the catalytic performance of group VIII base-metal catalysts, the subsequent study should aim at the more controllable synthesis of encapsulated Fe-, Co-, and Ni-based catalysts with fine structure in large-scale and better understanding on the inner mechanism of promotion effects derived from the encapsulation structures.

As mentioned above, the spatial restriction generated from the encapsulation structures has been proved to be effective to suppress the sintering of catalysts, which is one of the most important reasons for catalyst deactivation in chemical industries. However, the current synthesis of encapsulated catalysts is still in gram-scale, which is far away from the target of industrial applications. Thus, the large-scale synthesis of encapsulated catalysts is the essential criteria to lengthen the lifetime of Fe-, Co-, and Ni-based encapsulated catalysts in practical applications. Additionally, the materials used as coatings in the encapsulation structures are rather limited. Compared with SiO_2, carbon, and alumina, which are mostly utilized as the protective layer in the encapsulation structure at present, it is more attractive to synthesize the encapsulation structure with catalysis-assisting oxide (e.g., CeO_2, ZrO_2) coatings to strengthen the metal−support interaction. Metal catalysts encapsulated by graphene or a metal organic framework (MOF) have also drawn increasing attention.[221,222]

Moreover, there is a discrepancy between the prepared encapsulated catalysts and the ideal models due to the intrinsic defects in the real materials. Therefore, before the deeper investigation into the confinement effect, the synthesis of well-defined and tunable encapsulated catalysts (e.g., metal NPs with uniform size, selective shell thickness, and surface properties of the supports) is the prerequisite for deeper investigation into the confinement effect. Another focus in further work is the size control of the encapsulated structures. Most encapsulated catalysts involved in this review are at or above the several nanometer scale, which is not the maximum utilization of the metal atoms. When the size of metal NPs decreases to

DOI: 10.1021/acscatal.5b01221
ACS Catal. 2015, 5, 4959−4977

subnanometer or even single atom level, it possible to improve not only the efficiency of metal atom utilization but also the activity and selectivity of the catalysts.[223,224] One case in the encapsulated catalysts is the above-mentioned single Fe site confined in the SiO_2 matrix, which is exceptionally active in methane conversion.[22] The efforts to obtain encapsulated Fe-, Co-, and Ni-based catalysts with subnanometer or single atom metal cores is very promising to improve the catalytic performance of group VIII base-metal catalysts in the future. Another potential problem is that the mass transfer of the reactants and products would be restricted by the coating layer to some extent. Thus, the porosity of the coating layer should also be taken into account in the design of group VIII base-metal encapsulated catalysts.

The explanation and deep understanding on the improved catalytic performance induced by encapsulation structures remains elusive. As mentioned above, the Oswald ripening and particle migration are two different mass transport processes of sintering. The particle migration process could be prevented by introducing the complete encapsulation structures. However, the Oswald ripening, which happens through the migration of metal monomers in gas phase under some specific reaction conditions, might not be suppressed thoroughly by the introduction of encapsulation structures. The ability of encapsulation structures to alleviate the sintering resulting from Oswald ripening cannot be described accurately so far. Therefore, it is interesting to study how to quantify the degree of sintering-resistance caused by the encapsulated catalysts against the Oswald ripening process. Another problem is that the applications of encapsulation structures to promote the catalytic activity and selectivity are only reported on several specific cases. Although the promotion of catalytic activity induced by the confinement effect is attractive, it seems that the confinement effect is only the characteristic of the carbon materials with special electronic structure. The further extension of the confinement effect on more supports will provide a strong evidence on its universality. Multifunctional catalysts with encapsulation structure could serve as effective methods to achieve process intensification in catalytic reactions. However, the optimization on the composition and morphology of encapsulated multifunctional catalysts, which is crucial to obtain the compatibility between different steps in the reactions, still needs further study. In addition to the promotion in catalytic performance, the encapsulation structure is also a suitable model to study the metal−support interaction, which plays a significant role in the catalysis. For example, the well-defined core@shell structures could maximize the interaction between metal NPs and support. Therefore, the area of the interface between the metal and the support could be modulated facilely by changing the parameters of the core@shell structures. Moreover, an advanced characterization technique is the prerequisite to solve the above problem in relation to the mechanism of encapsulated catalysts.[225]

In conclusion, an understanding of the inner mechanism of encapsulated catalysts (e.g., the identification of active sites, size effects, electronic effects, interfacial effects) with enhanced catalytic properties would help us to design novel catalysts reasonably and predict the catalytic activity precisely in more reactions. Thus, further investigations including experimental and theoretical methods into the encapsulation structures are particularly essential in the near future. The investigations in encapsulated group VIII metal catalysts are promising for both academic developments and practical applications.

AUTHOR INFORMATION

Corresponding Author

*E-mail: jlgong@tju.edu.cn. Fax: +86-22-87401818.

Notes

The authors declare no competing financial interest.

ACKNOWLEDGMENTS

This work was supported by the National Natural Science Foundation of China (21206115, 21222604, and 21376169), the Program for New Century Excellent Talents in University (NCET-10-0611), the Scientific Research Foundation for the Returned Overseas Chinese Scholars (MoE), and the Program of Introducing Talents of Discipline to Universities (B06006).

REFERENCES

(1) Jia, C.-J.; Schuth, F. *Phys. Chem. Chem. Phys.* **2011**, *13*, 2457−2487.
(2) P. In *Catalysis from A to Z: A Concise Encyclopedia*, 4th ed.; Cornils, B., Herrmann, W. A., Zanthoff, H.-W., Wong, C.-H., Eds; Wiley-VCH Verlag GmbH & Co. KGaA: Weinheim, 2013; p 1782.
(3) R. In *Catalysis from A to Z: A Concise Encyclopedia*, 4th ed.; Cornils, B., Herrmann, W. A., Zanthoff, H.-W., Wong, C.-H., Eds; Wiley-VCH Verlag GmbH & Co. KGaA: Weinheim, 2013; p 1951.
(4) Pakhare, D.; Spivey, J. *Chem. Soc. Rev.* **2014**, *43*, 7813−7837.
(5) C. In *Catalysis from A to Z: A Concise Encyclopedia*, 4th ed.; Cornils, B., Herrmann, W. A., Zanthoff, H.-W., Wong, C.-H., Eds; Wiley-VCH Verlag GmbH & Co. KGaA: Weinheim, 2013; p 534.
(6) I. In *Catalysis from A to Z: A Concise Encyclopedia*, 4th ed.; Cornils, B., Herrmann, W. A., Zanthoff, H.-W., Wong, C.-H., Eds; Wiley-VCH Verlag GmbH & Co. KGaA: Weinheim, 2013; p 1248.
(7) N. *In Catalysis from A to Z: A Concise Encyclopedia*, 4th ed.; Cornils, B., Herrmann, W. A., Zanthoff, H.-W., Wong, C.-H., Eds; Wiley-VCH Verlag GmbH & Co. KGaA: Weinheim, 2013; p 1564.
(8) Fu, T.; Li, Z. *Chem. Eng. Sci.* **2015**, http://dx.doi.org/10.1016/j.ces.2015.03.007.
(9) Mattos, L. V.; Jacobs, G.; Davis, B. H.; Noronha, F. B. *Chem. Rev.* **2012**, *112*, 4094−4123.
(10) Wei, W.; Jinlong, G. *Front. Chem. Sci. Eng.* **2011**, *5*, 2−10.
(11) Liu, C.-j.; Ye, J.; Jiang, J.; Pan, Y. *ChemCatChem* **2011**, *3*, 529−541.
(12) Ratnasamy, C.; Wagner, J. P. *Catal. Rev.: Sci. Eng.* **2009**, *51*, 325−440.
(13) Xie, X.; Li, Y.; Liu, Z.-Q.; Haruta, M.; Shen, W. *Nature* **2009**, *458*, 746−749.
(14) Sehested, J.; Carlsson, A.; Janssens, T. V. W.; Hansen, P. L.; Datye, A. K. *J. Catal.* **2001**, *197*, 200−209.
(15) Sehested, J. *J. Catal.* **2003**, *217*, 417−426.
(16) Sehested, J.; Gelten, J. A. P.; Remediakis, I. N.; Bengaard, H.; Nørskov, J. K. *J. Catal.* **2004**, *223*, 432−443.
(17) De Rogatis, L.; Cargnello, M.; Gombac, V.; Lorenzut, B.; Montini, T.; Fornasiero, P. *ChemSusChem* **2010**, *3*, 24−42.
(18) Zhang, Z.-c.; Xu, B.; Wang, X. *Chem. Soc. Rev.* **2014**, *43*, 7870−7886.
(19) Zaera, F. *Chem. Soc. Rev.* **2013**, *42*, 2746−2762.
(20) Cao, A.; Lu, R.; Veser, G. *Phys. Chem. Chem. Phys.* **2010**, *12*, 13499−13510.
(21) Li, S.; Gong, J. *Chem. Soc. Rev.* **2014**, *43*, 7245−7256.
(22) Guo, X.; Fang, G.; Li, G.; Ma, H.; Fan, H.; Yu, L.; Ma, C.; Wu, X.; Deng, D.; Wei, M.; Tan, D.; Si, R.; Zhang, S.; Li, J.; Sun, L.; Tang, Z.; Pan, X.; Bao, X. *Science* **2014**, *344*, 616−619.
(23) Pan, X.; Bao, X. *Acc. Chem. Res.* **2011**, *44*, 553−562.
(24) Yang, F.; Deng, D.; Pan, X.; Fu, Q.; Bao, X. *Natl. Sci. Rev.* **2015**, *2*, 183−201.
(25) Fan, G.; Li, F.; Evans, D. G.; Duan, X. *Chem. Soc. Rev.* **2014**, *43*, 7040−7066.
(26) Peña, M. A.; Fierro, J. L. G. *Chem. Rev.* **2001**, *101*, 1981−2018.

DOI: 10.1021/acscatal.5b01221
ACS Catal. 2015, 5, 4959−4977

(27) Zhu, J.; Li, H.; Zhong, L.; Xiao, P.; Xu, X.; Yang, X.; Zhao, Z.; Li, J. *ACS Catal.* **2014**, *4*, 2917−2940.
(28) Zhang, Q.; Lee, I.; Joo, J. B.; Zaera, F.; Yin, Y. *Acc. Chem. Res.* **2012**, *46*, 1816−1824.
(29) Ghosh Chaudhuri, R.; Paria, S. *Chem. Rev.* **2011**, *112*, 2373−2433.
(30) Yin, Y.; Rioux, R. M.; Erdonmez, C. K.; Hughes, S.; Somorjai, G. A.; Alivisatos, A. P. *Science* **2004**, *304*, 711−714.
(31) Priebe, M.; Fromm, K. M. *Chem. - Eur. J.* **2015**, *21*, 3854−3874.
(32) Bao, J.; He, J.; Zhang, Y.; Yoneyama, Y.; Tsubaki, N. *Angew. Chem., Int. Ed.* **2008**, *47*, 353−356.
(33) Joo, S. H.; Park, J. Y.; Tsung, C.-K.; Yamada, Y.; Yang, P.; Somorjai, G. A. *Nat. Mater.* **2009**, *8*, 126−131.
(34) Zhang, C.; Li, S.; Wang, T.; Wu, G.; Ma, X.; Gong, J. *Chem. Commun.* **2013**, *49*, 10647−10649.
(35) Liu, S.; Han, M.-Y. *Chem. - Asian J.* **2010**, *5*, 36−45.
(36) Takenaka, S.; Umebayashi, H.; Tanabe, E.; Matsune, H.; Kishida, M. *J. Catal.* **2007**, *245*, 392−400.
(37) Takenaka, S.; Orita, Y.; Umebayashi, H.; Matsune, H.; Kishida, M. *Appl. Catal., A* **2008**, *351*, 189−194.
(38) Dahlberg, K. A.; Schwank, J. W. *Chem. Mater.* **2012**, *24*, 2635−2644.
(39) Stöber, W.; Fink, A.; Bohn, E. *J. Colloid Interface Sci.* **1968**, *26*, 62−69.
(40) Wong, Y. J.; Zhu, L.; Teo, W. S.; Tan, Y. W.; Yang, Y.; Wang, C.; Chen, H. *J. Am. Chem. Soc.* **2011**, *133*, 11422−11425.
(41) Li, W.; Zhao, D. *Adv. Mater.* **2013**, *25*, 142−149.
(42) Feyen, M.; Weidenthaler, C.; Güttel, R.; Schlichte, K.; Holle, U.; Lu, A.-H.; Schüth, F. *Chem. - Eur. J.* **2011**, *17*, 598−605.
(43) Li, L.; He, S.; Song, Y.; Zhao, J.; Ji, W.; Au, C.-T. *J. Catal.* **2012**, *288*, 54−64.
(44) Zhang, J.; Li, F. *Appl. Catal., B* **2015**, *176*−*177*, 513−521.
(45) Zeng, B.; Hou, B.; Jia, L.; Li, D.; Sun, Y. *J. Mol. Catal. A: Chem.* **2013**, *379*, 263−268.
(46) Zeng, B.; Hou, B.; Jia, L.; Wang, J.; Chen, C.; Li, D.; Sun, Y. *Catal. Sci. Technol.* **2013**, *3*, 3250−3255.
(47) Zeng, B.; Hou, B.; Jia, L.; Wang, J.; Chen, C.; Sun, Y.; Li, D. *ChemCatChem* **2013**, *5*, 3794−3801.
(48) Karandikar, P. R.; Lee, Y.-J.; Kwak, G.; Woo, M. H.; Park, S.-J.; Park, H.-G.; Ha, K.-S.; Jun, K.-W. *J. Phys. Chem. C* **2014**, *118*, 21975−21985.
(49) Li, Y.; Liu, S.; Yao, L.; Ji, W.; Au, C.-T. *Catal. Commun.* **2010**, *11*, 368−372.
(50) Park, J.; Song, H. *Nano Res.* **2011**, *4*, 33−49.
(51) Park, J. C.; Lee, H. J.; Kim, J. Y.; Park, K. H.; Song, H. *J. Phys. Chem. C* **2010**, *114*, 6381−6388.
(52) Li, Z.; Mo, L.; Kathiraser, Y.; Kawi, S. *ACS Catal.* **2014**, *4*, 1526−1536.
(53) Park, J. C.; Lee, H. J.; Jung, H. S.; Kim, M.; Kim, H. J.; Park, K. H.; Song, H. *ChemCatChem* **2011**, *3*, 755−760.
(54) Park, J. C.; Bang, J. U.; Lee, J.; Ko, C. H.; Song, H. *J. Mater. Chem.* **2010**, *20*, 1239−1246.
(55) Li, L.; Yao, Y.; Sun, B.; Fei, Z.; Xia, H.; Zhao, J.; Ji, W.; Au, C.-T. *ChemCatChem* **2013**, *5*, 3781−3787.
(56) Li, L.; Lu, P.; Yao, Y.; Ji, W. *Catal. Commun.* **2012**, *26*, 72−77.
(57) Li, Z.; Kathiraser, Y.; Ashok, J.; Oemar, U.; Kawi, S. *Langmuir* **2014**, *30*, 14694−14705.
(58) Mo, L.; Leong, K. K. M.; Kawi, S. *Catal. Sci. Technol.* **2014**, *4*, 2107−2114.
(59) Xie, R.; Wang, H.; Gao, P.; Xia, L.; Zhang, Z.; Zhao, T.; Sun, Y. *Appl. Catal., A* **2015**, *492*, 93−99.
(60) Sun, X.; Li, Y. *Angew. Chem., Int. Ed.* **2004**, *43*, 597−601.
(61) Yu, G.; Sun, B.; Pei, Y.; Xie, S.; Yan, S.; Qiao, M.; Fan, K.; Zhang, X.; Zong, B. *J. Am. Chem. Soc.* **2010**, *132*, 935−937.
(62) Yan, Q.; Wan, C.; Liu, J.; Gao, J.; Yu, F.; Zhang, J.; Cai, Z. *Green Chem.* **2013**, *15*, 1631−1640.
(63) Li, B.; Sun, B.; Qian, X.; Li, W.; Wu, Z.; Sun, Z.; Qiao, M.; Duke, M.; Zhao, D. *J. Am. Chem. Soc.* **2013**, *135*, 1181−1184.
(64) Zhang, J.; Zhang, X.; Tu, M.; Liu, W.; Liu, H.; Qiu, J.; Zhou, L.; Shao, Z.; Ho, H. L.; Yeung, K. L. *J. Power Sources* **2012**, *198*, 14−22.
(65) Zhang, J.; Zhang, X.; Liu, W.; Liu, H.; Qiu, J.; Yeung, K. L. *J. Power Sources* **2014**, *246*, 74−83.
(66) Xiao, J.; Pan, X.; Guo, S.; Ren, P.; Bao, X. *J. Am. Chem. Soc.* **2014**, *137*, 477−482.
(67) Pan, X.; Bao, X. *Chem. Commun.* **2008**, 6271−6281.
(68) Wang, C.; Guo, S.; Pan, X.; Chen, W.; Bao, X. *J. Mater. Chem.* **2008**, *18*, 5782−5786.
(69) Ajayan, P. M.; Ebbesen, T. W.; Ichihashi, T.; Iijima, S.; Tanigaki, K.; Hiura, H. *Nature* **1993**, *362*, 522−525.
(70) Guerret-Piecourt, C.; Bouar, Y. L.; Lolseau, A.; Pascard, H. *Nature* **1994**, *372*, 761−765.
(71) Ugarte, D.; Châtelain, A.; de Heer, W. A. *Science* **1996**, *274*, 1897−1899.
(72) Shiozawa, H.; Pichler, T.; Grüneis, A.; Pfeiffer, R.; Kuzmany, H.; Liu, Z.; Suenaga, K.; Kataura, H. *Adv. Mater.* **2008**, *20*, 1443−1449.
(73) Castillejos, E.; Debouttière, P.-J.; Roiban, L.; Solhy, A.; Martinez, V.; Kihn, Y.; Ersen, O.; Philippot, K.; Chaudret, B.; Serp, P. *Angew. Chem., Int. Ed.* **2009**, *48*, 2529−2533.
(74) Chen, W.; Pan, X.; Willinger, M.-G.; Su, D. S.; Bao, X. *J. Am. Chem. Soc.* **2006**, *128*, 3136−3137.
(75) Cao, F.; Zhong, K.; Gao, A.; Chen, C.; Li, Q.; Chen, Q. *J. Phys. Chem. B* **2007**, *111*, 1724−1728.
(76) Yuan, Q.; Yin, A.-X.; Luo, C.; Sun, L.-D.; Zhang, Y.-W.; Duan, W.-T.; Liu, H.-C.; Yan, C.-H. *J. Am. Chem. Soc.* **2008**, *130*, 3465−3472.
(77) Xing, C.; Yang, G.; Wang, D.; Zeng, C.; Jin, Y.; Yang, R.; Suehiro, Y.; Tsubaki, N. *Catal. Today* **2013**, *215*, 24−28.
(78) Trépanier, M.; Dalai, A. K.; Abatzoglou, N. *Appl. Catal., A* **2010**, *374*, 79−86.
(79) Zhang, H.; Alhamed, Y. A.; Chu, W.; Ye, Z.; AlZahrani, A.; Petrov, L. *Appl. Catal., A* **2013**, *464*−*465*, 156−164.
(80) Ma, Q.; Wang, D.; Wu, M.; Zhao, T.; Yoneyama, Y.; Tsubaki, N. *Fuel* **2013**, *108*, 430−438.
(81) Ziegler, K. J.; Gu, Z.; Peng, H.; Flor, E. L.; Hauge, R. H.; Smalley, R. E. *J. Am. Chem. Soc.* **2005**, *127*, 1541−1547.
(82) Tavasoli, A.; Abbaslou, R. M. M.; Trepanier, M.; Dalai, A. K. *Appl. Catal., A* **2008**, *345*, 134−142.
(83) Rodrigues, J. J.; Fernandes, F. A. N.; Rodrigues, M. G. F. *Appl. Catal., A* **2013**, *468*, 32−37.
(84) Pan, X.; Fan, Z.; Chen, W.; Ding, Y.; Luo, H.; Bao, X. *Nat. Mater.* **2007**, *6*, 507−511.
(85) Zhu, Y.; Ye, Y.; Zhang, S.; Leong, M. E.; Tao, F. *Langmuir* **2012**, *28*, 8275−8280.
(86) Chen, H.; Yang, Y.; Hu, Z.; Huo, K.; Ma, Y.; Chen, Y.; Wang, X.; Lu, Y. *J. Phys. Chem. B* **2006**, *110*, 16422−16427.
(87) Lu, J.; Yang, L.; Xu, B.; Wu, Q.; Zhang, D.; Yuan, S.; Zhai, Y.; Wang, X.; Fan, Y.; Hu, Z. *ACS Catal.* **2014**, *4*, 613−621.
(88) Gates, B. C. *Chem. Rev.* **1995**, *95*, 511−522.
(89) Iglesia, E.; Soled, S. L.; Fiato, R. A. *J. Catal.* **1992**, *137*, 212−224.
(90) Bartholomew, C. H.; Pannell, R. B.; Butler, J. L. *J. Catal.* **1980**, *65*, 335−347.
(91) Tessonnier, J.-P.; Ersen, O.; Weinberg, G.; Pham-Huu, C.; Su, D. S.; Schlögl, R. *ACS Nano* **2009**, *3*, 2081−2089.
(92) Zhang, C.; Zhu, W.; Li, S.; Wu, G.; Ma, X.; Wang, X.; Gong, J. *Chem. Commun.* **2013**, *49*, 9383−9385.
(93) Prieto, G.; Shakeri, M.; de Jong, K. P.; de Jongh, P. E. *ACS Nano* **2014**, *8*, 2522−2531.
(94) Munnik, P.; Velthoen, M. E. Z.; de Jongh, P. E.; de Jong, K. P.; Gommes, C. J. *Angew. Chem., Int. Ed.* **2014**, *53*, 9493−9497.
(95) Perego, C.; Millini, R. *Chem. Soc. Rev.* **2013**, *42*, 3956−3976.
(96) Linares, N.; Silvestre-Albero, A. M.; Serrano, E.; Silvestre-Albero, J.; Garcia-Martinez, J. *Chem. Soc. Rev.* **2014**, *43*, 7681−7717.
(97) Valange, S.; Palacio, R.; Charmot, A.; Barrault, J.; Louati, A.; Gabelica, Z. *J. Mol. Catal. A: Chem.* **2009**, *305*, 24−33.
(98) Gómez-Reynoso, R.; Ramírez, J.; Nares, R.; Luna, R.; Murrieta, F. *Catal. Today* **2005**, *107*−*108*, 926−932.
(99) Li, X.-K.; Ji, W.-J.; Zhao, J.; Wang, S.-J.; Au, C.-T. *J. Catal.* **2005**, *236*, 181−189.

DOI: 10.1021/acscatal.5b01221
ACS Catal. 2015, 5, 4959−4977

(100) Zhang, M.; Ji, S.; Hu, L.; Yin, F.; Li, C.; Liu, H. *Chin. J. Catal.* **2006**, *27*, 777−781.
(101) Liu, D.; Lau, R.; Borgna, A.; Yang, Y. *Appl. Catal., A* **2009**, *358*, 110−118.
(102) Liu, H.; Wang, H.; Shen, J.; Sun, Y.; Liu, Z. *Appl. Catal., A* **2008**, *337*, 138−147.
(103) Tsoncheva, T.; Ivanova, L.; Rosenholm, J.; Linden, M. *Appl. Catal., B* **2009**, *89*, 365−374.
(104) Yamamoto, K.; Sunagawa, Y.; Takahashi, H.; Muramatsu, A. *Chem. Commun.* **2005**, 348−350.
(105) Lopes, I.; El Hassan, N.; Guerba, H.; Wallez, G.; Davidson, A. *Chem. Mater.* **2006**, *18*, 5826−5828.
(106) van der Meer, J.; Bardez, I.; Bart, F.; Albouy, P.-A.; Wallez, G.; Davidson, A. *Microporous Mesoporous Mater.* **2009**, *118*, 183−188.
(107) Taghavimoghaddam, J.; Knowles, G. P.; Chaffee, A. L. *J. Mol. Catal. A: Chem.* **2012**, *358*, 79−88.
(108) van der Meer, J.; Bardez-Giboire, I.; Mercier, C.; Revel, B.; Davidson, A.; Denoyel, R. *J. Phys. Chem. C* **2010**, *114*, 3507−3515.
(109) Ungureanu, A.; Dragoi, B.; Chirieac, A.; Royer, S.; Duprez, D.; Dumitriu, E. *J. Mater. Chem.* **2011**, *21*, 12529−12541.
(110) Ungureanu, A.; Dragoi, B.; Chirieac, A.; Ciotonea, C.; Royer, S.; Duprez, D.; Mamede, A. S.; Dumitriu, E. *ACS Appl. Mater. Interfaces* **2013**, *5*, 3010−3025.
(111) Friedrich, H.; Sietsma, J. R. A.; de Jongh, P. E.; Verkleij, A. J.; de Jong, K. P. *J. Am. Chem. Soc.* **2007**, *129*, 10249−10254.
(112) Sietsma, J. R. A.; Meeldijk, J. D.; den Breejen, J. P.; Versluijs-Helder, M.; van Dillen, A. J.; de Jongh, P. E.; de Jong, K. P. *Angew. Chem., Int. Ed.* **2007**, *46*, 4547−4549.
(113) Sietsma, J. R. A.; Meeldijk, J. D.; Versluijs-Helder, M.; Broersma, A.; Dillen, A. J. v.; de Jongh, P. E.; de Jong, K. P. *Chem. Mater.* **2008**, *20*, 2921−2931.
(114) Wolters, M.; Munnik, P.; Bitter, J. H.; de Jongh, P. E.; de Jong, K. P. *J. Phys. Chem. C* **2011**, *115*, 3332−3339.
(115) Munnik, P.; de Jongh, P. E.; de Jong, K. P. *J. Am. Chem. Soc.* **2014**, *136*, 7333−7340.
(116) Xie, T.; Shi, L.; Zhang, J.; Zhang, D. *Chem. Commun.* **2014**, *50*, 7250−7253.
(117) Liu, D.; Quek, X. Y.; Cheo, W. N. E.; Lau, R.; Borgna, A.; Yang, Y. *J. Catal.* **2009**, *266*, 380−390.
(118) Quek, X.-Y.; Liu, D.; Cheo, W. N. E.; Wang, H.; Chen, Y.; Yang, Y. *Appl. Catal., B* **2010**, *95*, 374−382.
(119) Liu, Z.; Zhou, J.; Cao, K.; Yang, W.; Gao, H.; Wang, Y.; Li, H. *Appl. Catal., B* **2012**, *125*, 324−330.
(120) Li, D.; Zeng, L.; Li, X.; Zhang, C.; Wang, X.; Ma, H.; Assabumrungrat, S.; Gong, J. *Appl. Catal., B* **2015**, *176*−*177*, 532−541.
(121) Zhang, S.; Muratsugu, S.; Ishiguro, N.; Tada, M. *ACS Catal.* **2013**, *3*, 1855−1864.
(122) Zhao, Y.; Zhang, Y.; Chen, J.; Li, J.; Liew, K.; Nordin, M. R. B. *ChemCatChem* **2012**, *4*, 265−272.
(123) Wang, N.; Shen, K.; Yu, X.; Qian, W.; Chu, W. *Catal. Sci. Technol.* **2013**, *3*, 2278−2287.
(124) Čejka, J. *Appl. Catal., A* **2003**, *254*, 327−338.
(125) Casey, W. H. *Chem. Rev.* **2005**, *106*, 1−16.
(126) Li, Z.-X.; Shi, F.-B.; Li, L.-L.; Zhang, T.; Yan, C.-H. *Phys. Chem. Chem. Phys.* **2011**, *13*, 2488−2491.
(127) Subramanian, V.; Gnanakumar, E. S.; Jeong, D.-W.; Han, W.-B.; Gopinath, C. S.; Roh, H.-S. *Chem. Commun.* **2013**, *49*, 11257−11259.
(128) Morris, S. M.; Fulvio, P. F.; Jaroniec, M. *J. Am. Chem. Soc.* **2008**, *130*, 15210−15216.
(129) Xu, L.; Song, H.; Chou, L. *Catal. Sci. Technol.* **2011**, *1*, 1032−1042.
(130) Tao, K.; Shi, L.; Ma, Q.; Wang, D.; Zeng, C.; Kong, C.; Wu, M.; Chen, L.; Zhou, S.; Hu, Y.; Tsubaki, N. *Chem. Eng. J.* **2013**, *221*, 25−31.
(131) Horiguchi, J.; Kobayashi, Y.; Kobayashi, S.; Yamazaki, Y.; Omata, K.; Nagao, D.; Konno, M.; Yamada, M. *Appl. Catal., A* **2011**, *392*, 86−92.
(132) Tian, H.; Li, S.; Zeng, L.; Ma, H.; Gong, J. *Sci. China Mater.* **2015**, *58*, 9−15.
(133) Shen, W.; Komatsubara, K.; Hagiyama, T.; Yoshida, A.; Naito, S. *Chem. Commun.* **2009**, 6490−6492.
(134) Xu, L.; Song, H.; Chou, L. *Appl. Catal., B* **2011**, *108*−*109*, 177−190.
(135) Xu, L.; Song, H.; Chou, L. *ACS Catal.* **2012**, *2*, 1331−1342.
(136) Xu, L.; Miao, Z.; Song, H.; Chen, W.; Chou, L. *Catal. Sci. Technol.* **2014**, *4*, 1759−1770.
(137) Wang, N.; Shen, K.; Huang, L.; Yu, X.; Qian, W.; Chu, W. *ACS Catal.* **2013**, *3*, 1638−1651.
(138) Wang, N.; Xu, Z.; Deng, J.; Shen, K.; Yu, X.; Qian, W.; Chu, W.; Wei, F. *ChemCatChem* **2014**, *6*, 1470−1480.
(139) Liu, Q.; Gao, J.; Gu, F.; Lu, X.; Liu, Y.; Li, H.; Zhong, Z.; Liu, B.; Xu, G.; Su, F. *J. Catal.* **2015**, *326*, 127−138.
(140) Chen, A.; Miyao, T.; Higashiyama, K.; Yamashita, H.; Watanabe, M. *Angew. Chem., Int. Ed.* **2010**, *49*, 9895−9898.
(141) Shang, X.; Wang, X.; Nie, W.; Guo, X.; Zou, X.; Ding, W.; Lu, X. *J. Mater. Chem.* **2012**, *22*, 23806−23814.
(142) Tan, M.; Wang, X.; Shang, X.; Zou, X.; Lu, X.; Ding, W. *J. Catal.* **2014**, *314*, 117−131.
(143) Tan, M.; Wang, X.; Wang, X.; Zou, X.; Ding, W.; Lu, X. *J. Catal.* **2015**, *329*, 151−166.
(144) Liang, C.; Li, Z.; Dai, S. *Angew. Chem., Int. Ed.* **2008**, *47*, 3696−3717.
(145) Geng, L.; Zhang, X.; Zhang, W.; Jia, M.; Liu, G. *Chem. Commun.* **2014**, *50*, 2965−2967.
(146) Ha, K.-S.; Kwak, G.; Jun, K.-W.; Hwang, J.; Lee, J. *Chem. Commun.* **2013**, *49*, 5141−5143.
(147) Lu, A.-H.; Nitz, J.-J.; Comotti, M.; Weidenthaler, C.; Schlichte, K.; Lehmann, C. W.; Terasaki, O.; Schüth, F. *J. Am. Chem. Soc.* **2010**, *132*, 14152−14162.
(148) Wu, Z.; Li, W.; Webley, P. A.; Zhao, D. *Adv. Mater.* **2012**, *24*, 485−491.
(149) Sun, Z.; Sun, B.; Qiao, M.; Wei, J.; Yue, Q.; Wang, C.; Deng, Y.; Kaliaguine, S.; Zhao, D. *J. Am. Chem. Soc.* **2012**, *134*, 17653−17660.
(150) Yang, Y.; Jia, L.; Hou, B.; Li, D.; Wang, J.; Sun, Y. *J. Phys. Chem. C* **2014**, *118*, 268−277.
(151) Yang, Y.; Jia, L.; Hou, B.; Li, D.; Wang, J.; Sun, Y. *ChemCatChem* **2014**, *6*, 319−327.
(152) Li, S.; Zhang, C.; Huang, Z.; Wu, G.; Gong, J. *Chem. Commun.* **2013**, *49*, 4226−4228.
(153) Sun, N.; Wen, X.; Wang, F.; Wei, W.; Sun, Y. *Energy Environ. Sci.* **2010**, *3*, 366−369.
(154) Seipenbusch, M.; Binder, A. *J. Phys. Chem. C* **2009**, *113*, 20606−20610.
(155) Lu, J.; Fu, B.; Kung, M. C.; Xiao, G.; Elam, J. W.; Kung, H. H.; Stair, P. C. *Science* **2012**, *335*, 1205−1208.
(156) O'Neill, B.; Jackson, D. H. K.; Lee, J.; Canlas, C.; Stair, P. C.; Marshall, C. L.; Elam, J. W.; Kuech, T. F.; Dumesic, J. A.; Huber, G. W. *ACS Catal.* **2015**, *5*, 1804−1825.
(157) Ma, Z.; Brown, S.; Howe, J. Y.; Overbury, S. H.; Dai, S. *J. Phys. Chem. C* **2008**, *112*, 9448−9457.
(158) Liang, X.; Li, J.; Yu, M.; McMurray, C. N.; Falconer, J. L.; Weimer, A. W. *ACS Catal.* **2011**, *1*, 1162−1165.
(159) Lu, J.; Elam, J. W.; Stair, P. C. *Acc. Chem. Res.* **2013**, *46*, 1806−1815.
(160) Kim, D. H.; Kim, S. Y.; Han, S. W.; Cho, Y. K.; Jeong, M.-G.; Park, E. J.; Kim, Y. D. *Appl. Catal., A* **2015**, *495*, 184−191.
(161) Kim, D.; Kim, K.-D.; Seo, H.; Dey, N.; Kim, M.; Kim, Y.; Lim, D.; Lee, K. *Catal. Lett.* **2011**, *141*, 854−859.
(162) Seo, H. O.; Sim, J. K.; Kim, K.-D.; Kim, Y. D.; Lim, D. C.; Kim, S. H. *Appl. Catal., A* **2013**, *451*, 43−49.
(163) Lee, J.; Jackson, D. H. K.; Li, T.; Winans, R. E.; Dumesic, J. A.; Kuech, T. F.; Huber, G. W. *Energy Environ. Sci.* **2014**, *7*, 1657−1660.
(164) Gould, T. D.; Izar, A.; Weimer, A. W.; Falconer, J. L.; Medlin, J. W. *ACS Catal.* **2014**, *4*, 2714−2717.

DOI: 10.1021/acscatal.5b01221
ACS Catal. 2015, 5, 4959−4977

(165) Gould, T. D.; Lubers, A. M.; Neltner, B. T.; Carrier, J. V.; Weimer, A. W.; Falconer, J. L.; Will Medlin, J. *J. Catal.* **2013**, *303*, 9−15.
(166) Gould, T. D.; Montemore, M. M.; Lubers, A. M.; Ellis, L. D.; Weimer, A. W.; Falconer, J. L.; Medlin, J. W. *Appl. Catal., A* **2015**, *492*, 107−116.
(167) Zeng, H. C. *Acc. Chem. Res.* **2012**, *46*, 226−235.
(168) Schauermann, S.; Nilius, N.; Shaikhutdinov, S.; Freund, H.-J. *Acc. Chem. Res.* **2012**, *46*, 1673−1681.
(169) Murzin, D. Y. *Langmuir* **2009**, *26*, 4854−4859.
(170) Campbell, C. T.; Parker, S. C.; Starr, D. E. *Science* **2002**, *298*, 811−814.
(171) Campbell, C. T. *Acc. Chem. Res.* **2013**, *46*, 1712−1719.
(172) Forzatti, P.; Lietti, L. *Catal. Today* **1999**, *52*, 165−181.
(173) Wynblatt, P.; Gjostein, N. A. *Prog. Solid State Chem.* **1975**, *9*, 21−58.
(174) Harris, P. J. F. *Int. Mater. Rev.* **1995**, *40*, 97−115.
(175) Ouyang, R.; Liu, J.-X.; Li, W.-X. *J. Am. Chem. Soc.* **2012**, *135*, 1760−1771.
(176) Moulijn, J. A.; van Diepen, A. E.; Kapteijn, F. *Appl. Catal., A* **2001**, *212*, 3−16.
(177) Datye, A. K.; Xu, Q.; Kharas, K. C.; McCarty, J. M. *Catal. Today* **2006**, *111*, 59−67.
(178) Challa, S. R.; Delariva, A. T.; Hansen, T. W.; Helveg, S.; Sehested, J.; Hansen, P. L.; Garzon, F.; Datye, A. K. *J. Am. Chem. Soc.* **2011**, *133*, 20672−20675.
(179) Hansen, T. W.; DeLaRiva, A. T.; Challa, S. R.; Datye, A. K. *Acc. Chem. Res.* **2013**, *46*, 1720−1730.
(180) DeLaRiva, A. T.; Hansen, T. W.; Challa, S. R.; Datye, A. K. *J. Catal.* **2013**, *308*, 291−305.
(181) Bezemer, G. L.; Remans, T. J.; van Bavel, A. P.; Dugulan, A. I. *J. Am. Chem. Soc.* **2010**, *132*, 8540−8541.
(182) Claeys, M.; Dry, M. E.; van Steen, E.; van Berge, P. J.; Booyens, S.; Crous, R.; van Helden, P.; Labuschagne, J.; Moodley, D. J.; Saib, A. M. *ACS Catal.* **2015**, *5*, 841−852.
(183) Sehested, J.; Larsen, N. W.; Falsig, H.; Hinnemann, B. *Catal. Today* **2014**, *228*, 22−31.
(184) Mirodatos, C.; Praliaud, H.; Primet, M. *J. Catal.* **1987**, *107*, 275−287.
(185) Mihaylov, M.; Hadjiivanov, K.; Knözinger, H. *Catal. Lett.* **2001**, *76*, 59−63.
(186) Ruban, A.; Hammer, B.; Stoltze, P.; Skriver, H. L.; Nørskov, J. K. *J. Mol. Catal. A: Chem.* **1997**, *115*, 421−429.
(187) Hammer, B.; Hansen, L. B.; Nørskov, J. K. *Phys. Rev. B: Condens. Matter Mater. Phys.* **1999**, *59*, 7413−7421.
(188) Hammer, B.; Nørskov, J. K. *Surf. Sci.* **1995**, *343*, 211−220.
(189) Mojet, B. L.; Miller, J. T.; Ramaker, D. E.; Koningsberger, D. C. *J. Catal.* **1999**, *186*, 373−386.
(190) Ramaker, D. E.; de Graaf, J.; van Veen, J. A. R.; Koningsberger, D. C. *J. Catal.* **2001**, *203*, 7−17.
(191) van de Loosdrecht, J.; van der Kraan, A. M.; van Dillen, A. J.; Geus, J. W. *J. Catal.* **1997**, *170*, 217−226.
(192) Stakheev, A. Y.; Kustov, L. M. *Appl. Catal., A* **1999**, *188*, 3−35.
(193) Serp, P.; Castillejos, E. *ChemCatChem* **2010**, *2*, 41−47.
(194) Odom, T. W.; Huang, J.-L.; Kim, P.; Lieber, C. M. *J. Phys. Chem. B* **2000**, *104*, 2794−2809.
(195) Planeix, J. M.; Coustel, N.; Coq, B.; Brotons, V.; Kumbhar, P. S.; Dutartre, R.; Geneste, P.; Bernier, P.; Ajayan, P. M. *J. Am. Chem. Soc.* **1994**, *116*, 7935−7936.
(196) Collins, P. G.; Bradley, K.; Ishigami, M.; Zettl, A. *Science* **2000**, *287*, 1801−1804.
(197) Chen, W.; Fan, Z.; Pan, X.; Bao, X. *J. Am. Chem. Soc.* **2008**, *130*, 9414−9419.
(198) Zhang, F.; Pan, X.; Hu, Y.; Yu, L.; Chen, X.; Jiang, P.; Zhang, H.; Deng, S.; Zhang, J.; Bolin, T. B.; Zhang, S.; Huang, Y.; Bao, X. *Proc. Natl. Acad. Sci. U. S. A.* **2013**, *110*, 14861−14866.
(199) Chen, W.; Pan, X.; Bao, X. *J. Am. Chem. Soc.* **2007**, *129*, 7421−7426.
(200) Yu, L.; Li, W.-X.; Pan, X.; Bao, X. *J. Phys. Chem. C* **2012**, *116*, 16461−16466.
(201) Yang, Z.; Guo, S.; Pan, X.; Wang, J.; Bao, X. *Energy Environ. Sci.* **2011**, *4*, 4500−4503.
(202) Davari, M.; Karimi, S.; Tavasoli, A.; Karimi, A. *Appl. Catal., A* **2014**, *485*, 133−142.
(203) Yang, H.; Song, S.; Rao, R.; Wang, X.; Yu, Q.; Zhang, A. *J. Mol. Catal. A: Chem.* **2010**, *323*, 33−39.
(204) Zhang, J.; Müller, J.-O.; Zheng, W.; Wang, D.; Su, D.; Schlögl, R. *Nano Lett.* **2008**, *8*, 2738−2743.
(205) Dautzenberg, F. M.; Mukherjee, M. *Chem. Eng. Sci.* **2001**, *56*, 251−267.
(206) Dietrich, W.; Lawrence, P. S.; Grünewald, M.; Agar, D. W. *Chem. Eng. J.* **2005**, *107*, 103−111.
(207) Gunn, D. J.; Thomas, W. J. *Chem. Eng. Sci.* **1965**, *20*, 89−100.
(208) Wu, G.; Zhang, C.; Li, S.; Huang, Z.; Yan, S.; Wang, S.; Ma, X.; Gong, J. *Energy Environ. Sci.* **2012**, *5*, 8942−8949.
(209) Yang, G.; Tsubaki, N.; Shamoto, J.; Yoneyama, Y.; Zhang, Y. *J. Am. Chem. Soc.* **2010**, *132*, 8129−8136.
(210) Sartipi, S.; Makkee, M.; Kapteijn, F.; Gascon, J. *Catal. Sci. Technol.* **2014**, *4*, 893−907.
(211) Abelló, S.; Montané, D. *ChemSusChem* **2011**, *4*, 1538−1556.
(212) Kruse, N.; Machoke, A. G.; Schwieger, W.; Güttel, R. *ChemCatChem* **2015**, *7*, 1018−1022.
(213) Sartipi, S.; Parashar, K.; Valero-Romero, M. J.; Santos, V. P.; van der Linden, B.; Makkee, M.; Kapteijn, F.; Gascon, J. *J. Catal.* **2013**, *305*, 179−190.
(214) Sartipi, S.; van Dijk, J. E.; Gascon, J.; Kapteijn, F. *Appl. Catal., A* **2013**, *456*, 11−22.
(215) He, J.; Liu, Z.; Yoneyama, Y.; Nishiyama, N.; Tsubaki, N. *Chem. - Eur. J.* **2006**, *12*, 8296−8304.
(216) Bao, J.; Yang, G.; Okada, C.; Yoneyama, Y.; Tsubaki, N. *Appl. Catal., A* **2011**, *394*, 195−200.
(217) Sun, B.; Yu, G.; Lin, J.; Xu, K.; Pei, Y.; Yan, S.; Qiao, M.; Fan, K.; Zhang, X.; Zong, B. *Catal. Sci. Technol.* **2012**, *2*, 1625−1629.
(218) Guan, J.; Pan, X.; Liu, X.; Bao, X. *J. Phys. Chem. C* **2009**, *113*, 21687−21692.
(219) Neal, L. M.; Shafiefarhood, A.; Li, F. *ACS Catal.* **2014**, *4*, 3560−3569.
(220) Mihai, O.; Chen, D.; Holmen, A. *J. Catal.* **2012**, *293*, 175−185.
(221) Wu, Z.-S.; Yang, S.; Sun, Y.; Parvez, K.; Feng, X.; Müllen, K. *J. Am. Chem. Soc.* **2012**, *134*, 9082−9085.
(222) Choi, K. M.; Na, K.; Somorjai, G. A.; Yaghi, O. M. *J. Am. Chem. Soc.* **2015**, *137*, 7810−7816.
(223) Qiao, B.; Wang, A.; Yang, X.; Allard, L. F.; Jiang, Z.; Cui, Y.; Liu, J.; Li, J.; Zhang, T. *Nat. Chem.* **2011**, *3*, 634−641.
(224) Yang, X.-F.; Wang, A.; Qiao, B.; Li, J.; Liu, J.; Zhang, T. *Acc. Chem. Res.* **2013**, *46*, 1740−1748.
(225) Zhang, Y.; Weng, X.; Li, H.; Li, H.; Wei, M.; Xiao, J.; Liu, Z.; Chen, M.; Fu, Q.; Bao, X. *Nano Lett.* **2015**, *15*, 3616−3623.

DOI: 10.1021/acscatal.5b01221
ACS Catal. 2015, 5, 4959−4977